Journal of the Iranian Chemical Society (2022) 19:1015–1038
https://doi.org/10.1007/s13738-021-02401-x

ORIGINAL PAPER

Synthesis, Antioxidant Activity, Spectroscopic, Electronic, Nonlinear Optical (NLO) and Thermodynamic Properties of 2-Ethoxy-4-[(5-oxo-3-phenyl-1,5-dihydro-1,2,4-triazol-4-ylimino)-methyl]-phenyl -4-methoxybenzoate: A Theoretical and Experimental Study

Hilal Medetalibeyoglu[1]

Received: 11 April 2021 / Accepted: 9 September 2021 / Published online: 2 October 2021

Abstract
In the present study, the synthesis, antioxidant activity, spectroscopic, electronic, and thermodynamic properties of 2-ethoxy-4-[(5-oxo-3-phenyl-1,5-dihydro-1,2,4-triazol-4-ylimino)-methyl]-phenyl-4-methoxybenzoate (EPM) were examined. The novel 2-ethoxy-4-[(5-oxo-3-phenyl-1,5-dihydro-1,2,4-triazol-4-ylimino)-methyl]-phenyl-4-methoxybenzoate (EPM) compound was successfully synthesized with novel derived biologically important 1,2,4-triazole Schiff base. This biologically active 1,2,4-triazole Schiff base was obtained through condensation of 3-phenyl-4-amino-4,5-dihydro-1*H*-1,2,4-triazol-5-one with 2-ethoxy-4-formylphenyl-4-methoxybenzoate. The characterization of the obtained compound was identified utilizing FT-IR, UV–Vis, ^{1}H-, and ^{13}C-NMR spectroscopies. The antioxidant activities of the newly synthesized Schiff base were evaluated employing the Oyaizu, Dinis, and Blois techniques. The optimized molecular structure, vibrational frequencies, ultraviolet–visible spectrums, and nuclear magnetic resonance values of the newly synthesized Schiff base were assessed through the use of density functional theory (DFT) with standard B3LYP/6–311++G(d,p) level. The harmonic vibration peaks were performed via comparison of the scaled values with the experimental FT-IR spectrum. The nuclear magnetic resonance chemical shift values were determined by the gauge-independent atomic orbital (GIAO) method. The nuclear magnetic resonance chemical shift values of the newly synthesized Schiff base in various solvents were examined at B3LYP/6–311++G(d,p) level utilizing integral equation formalism polarizable continuum model (IEFPCM). The chemical shift values of EPM were computed and compared with experimental findings. The correlational analysis (R^2) and RMSD results were evaluated to demonstrate correction and accuracy between calculated and experimental parameters. The HOMO–LUMO orbital forms and their energies were determined. The molecular electrostatic potential (MEP), Mulliken atomic charges, electronic absorption maximum wavelengths, thermodynamic characteristics (i.e., entropy, thermal capacity, and enthalpy), and nonlinear optical (NLO) properties (i.e., the first hyperpolarizability and polarizability) of the newly synthesized Schiff base were investigated. The correlational analysis results indicated a strong relationship between experimental and theoretical findings. The metal chelating activity of the newly synthesized Schiff base and standards was observed to decrease in the order of EDTA > EPM > α-tocopherol according to Dinis method. The newly synthesized Schiff base displayed such a good NLO property that it was 34 times as great as the property of urea. As a result, this chromophore could be a potential building block for nonlinear optical materials.

✉ Hilal Medetalibeyoglu
hilalmedet@gmail.com

[1] Chemistry Department, Faculty of Arts and Science, Kafkas University, 36100 Kars, Turkey

Graphic abstract

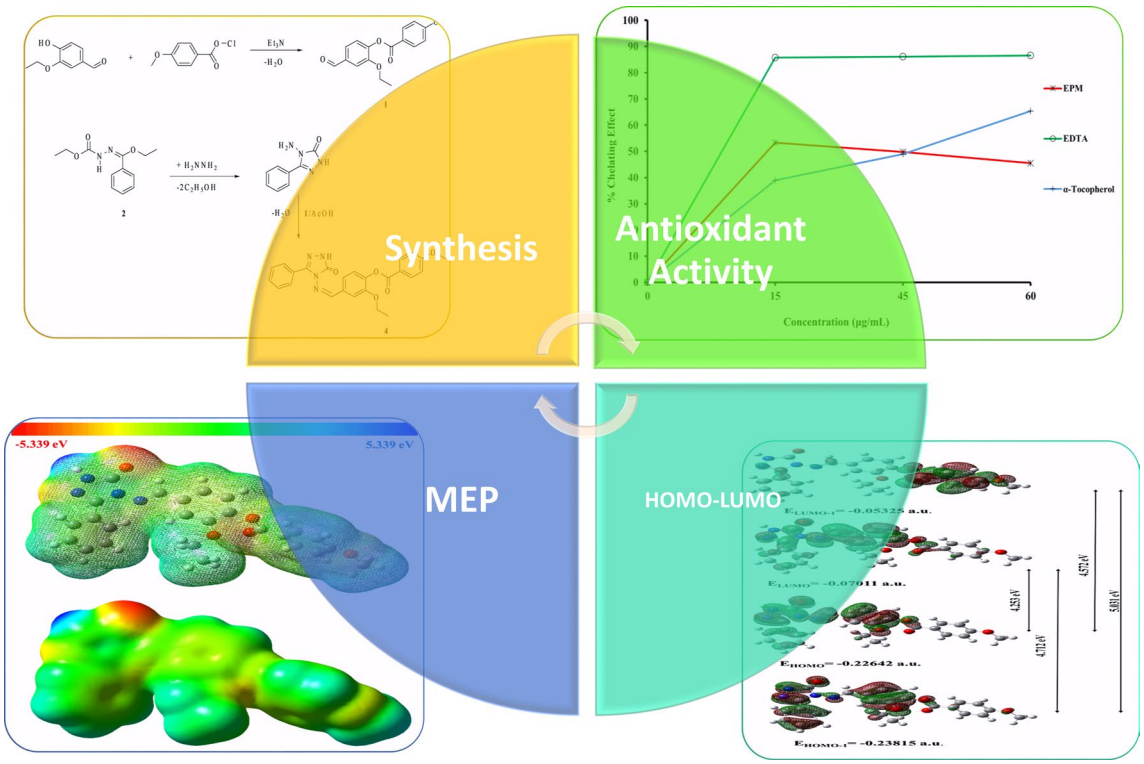

Keywords 1*H*-1,2,4-triazole derivatives · Synthesis · In vitro antioxidant activity · FT-IR · ^{1}H and ^{13}C NMR chemical shifts · DFT/B3LYP method

Introduction

Triazole moieties, especially 1,2,4-triazole and 4-amino-5-substituted 1,2,4-triazole, have several interesting properties in various fields such as biological and potential energy materials [1–3]. It was reported that 1,2,4-triazole Schiff base compounds could be antibacterial, anticancer, antifungal, anti-HIV, anti-inflammatory, anticonvulsant, antitumor, anti-tubercular, antiviral, antihypertensive agents known in the literature [4–8]. They are also well known for their remarkable antioxidant properties. A group of researchers investigated the antioxidant activity of some 1,2,4-triazole Schiff base compounds and discovered them to be strong antioxidants. This is because those compounds have the most potent biological role, which is probably due to the heteroatoms and/or azomethine linkage. Additionally, some compounds that contain 1,2,4-triazole ring have rather unusual structures and magnetic characteristics. These compounds are multifunctional ligands, and the coordination compounds produced from them are regarded as model systems for metal–ligand interactions reported in biological systems [9–11].

Quantum chemical calculations are frequently used to evaluate, comprehend, and predict experimental parameters such as ^{1}H, and ^{13}C chemical shift values, X-ray geometrical data, absorption/emission, and FT-IR, spectra. Recent developments in this field have led to a renewed interest in quantum chemical calculations and spectroscopic analysis to determine the relationship between these compounds' molecular structure and biological activity [12–15]. Furthermore, density functional theory (DFT) has become one of the most extensively employed theories in quantum chemical calculations in recent years [16–18]. By improving exchange–correlation functionals, it has been possible to calculate a large number of molecular properties with accuracy comparable to that of standard correlated ab initio approaches; all of this can be accomplished at a lower computing cost. During the literature review, it was determined that DFT has a high degree of precision in reproducing experimental data in geometrical parameters, vibrational frequency, dipole moment, and nuclear magnetic resonance value [19–22]. In this respect, DFT approaches have been used in investigating quantum chemical calculations of large organic molecules,

organometallic compounds, and metal complexes in all cases where electron correlation contributions were not negligible [23, 24].

Until recently, no previous study has investigated synthesis, antioxidant activity, quantum chemical calculations, and spectroscopic analysis of a novel 2-ethoxy-4-[(5-oxo-3-phenyl-1,5-dihydro-1,2,4-triazol-4-ylimino)-methyl]-phenyl-4-methoxybenzoate (EPM). In the light of those mentioned so far, the findings obtained from the studies prompted us to synthesize, characterize, study antioxidant activity and do quantum chemical calculations a novel Schiff base compound (EPM). Herein, 2-ethoxy-4-[(5-oxo-3-phenyl-1,5-dihydro-1,2,4-triazol-4-ylimino)-methyl]-phenyl-4-methoxybenzoate (EPM) was successfully synthesized in high yield 1,2,4-triazole-based Schiff base compound which were synthesized simply in a one-step condensation reaction between 3-phenyl-4-amino-4,5-dihydro-1*H*-1,2,4-triazol-5-one and 2-ethoxy-4-formylphenyl-4-methoxybenzoate. Based on the above facts, in the first section of this paper, the synthesis and antioxidant activity of 2-ethoxy-4-[(5-oxo-3-phenyl-1,5-dihydro-1,2,4-triazol-4-ylimino)-methyl]-phenyl-4-methoxybenzoate (EPM) will be examined. Throughout this section, first of all, the fact that 2-ethoxy-4-[(5-oxo-3-phenyl-1,5-dihydro-1,2,4-triazol-4-ylimino)-methyl]-phenyl-4-methoxybenzoate (EPM) was synthesized by using compounds 1 and 3 with the reaction of 3-phenyl-4-amino-4,5-dihydro-1*H*-1,2,4-triazol-5-one with 2-ethoxy-4-formylphenyl-4-methoxybenzoate. The next section begins by laying out the theoretical dimensions of the research and presents the findings. On the other hand, in this section, the information regarding the way through which the investigation of the molecular structure, $^{1}H/^{13}C$-NMR spectra, vibrational assignments, atomic charges, electronic absorption, molecular electrostatic potential (MEP), energy potential surface (PES), thermodynamic features (i.e., entropy, thermal capacity, and enthalpy), and nonlinear optical (NLO) properties (i.e., the first hyperpolarizability and polarizability) of EPM are conducted by B3LYP/6–311++G(d,p) level. The results of the structural, spectroscopic, thermodynamic, and electronic parameters are detailed herein. The study intends to contribute to this growing area of research by providing insight into synthesis, antioxidant activity, molecular, and spectral properties of EPM. The linear polarizability (α), the first hyperpolarizability (β), and dipole moment (μ) were calculated, and these results showed the title compound was a good candidate for a nonlinear optical material.

Experimental details

Materials and synthesis of the sample

In accordance with the aims of the study, chemical reagents and the solvents in the study were purchased from Merck AG, Aldrich, and Fluka. Scheme 1 presents the synthesis route on 2-ethoxy-4-[(5-oxo-3-phenyl-1,5-dihydro-1,2,4-triazol-4-ylimino)-methyl]-phenyl-4-methoxybenzoate (EPM) which was obtained through condensation reaction

Scheme 1 Syntheses route of compound **4**

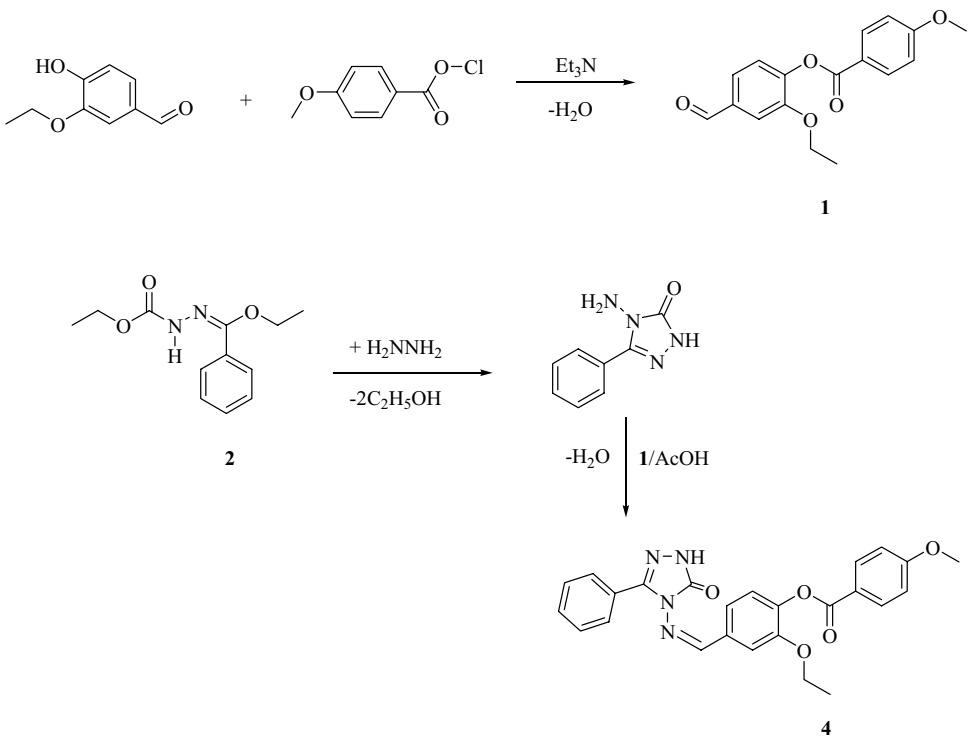

of 4-amino-5-phenyl-2*H*-1,2,4-triazol-3(4*H*)-one **3** with 2-ethoxy-4-formylphenyl-4-methoxybenzoate **1**. In the meantime, sample 1 was prepared in the following way: the solution of 3-ethoxy-4-hydroxybenzaldehyde (1 mmol) in ethyl acetate (20 mL) treated with 4-methoxybenzoyl chloride (1 mmol) was slowly added triethylamine (0.01 mol) by stirring at 0–5 °C. After two hours of stirring, the mixture was refluxed for three hours. It was then cooled and filtered. The filtrate evaporated *in vacuo*, and the crude product was washed with water and purified through recrystallization in ethanol to afford compound **1.** Later, compound **3** (1 mmol) was solved in acetic acid (20 mL) and handled with 2-ethoxy-4-formylphenyl-4-methoxybenzoate **1** (1 mmol), and the mixture was refluxed for two hours, followed by refluxing *in vacuo*, and then evaporated at 50–55 °C. The solid product was obtained and purified as colorless crystals by recrystallization in a small amount of ethanol to yield a novel Schiff base, 2-ethoxy-4-[(5-oxo-3-phenyl-1,5-dihydro-1,2,4-triazol-4-ylimino)-methyl]-phenyl-4-methoxybenzoate (4).

2-Ethoxy-4-[(5-oxo-3-phenyl-1,5-dihydro-1,2,4-triazol-4-ylimino)-methyl]-phenyl-4-methoxybenzoate (4) White solid; yield: Yield 4.52 g (98.71%). mp. 194 ºC. IR (KBr) ν 3160 (NH), 1732, 1687 (C=O), 1610 (C=N), 1260 (COO), 851 cm^{-1} (1,4 disubstituted benzenoid ring); ^{1}H NMR (200 MHz, DMSO-d_6) δ 1.22 (t, 3H, $OCH_2C\underline{H}_3$, J = 7.20 Hz), 3.88 (s, 3H, OCH_3), 4.09 (q, 2H, $OC\underline{H}_2CH_3$, J = 7.20 Hz), 7.13 (d, 2H, Ar–H, J = 8.80 Hz), 7.37 (d, 1H, Ar–H, J = 8.00 Hz), 7.47 (dd, 1H, Ar–H, J = 8.00, 1.60 Hz), 7.53–7.56 (m, 3H, Ar–H), 7.60 (d, 1H, Ar–H, J = 1.60 Hz), 7.93–7.95 (m, 2H, Ar–H), 8.09 (d, 2H, Ar–H, J = 8.80 Hz), 9.69 (s, 1H, N=CH), 12.42 (s, 1H, NH); ^{13}C NMR (50 MHz, DMSO-d_6) δ 14.32 ($OCH_2\underline{C}H_3$), 55.56 (OCH_3), 64.02 ($O\underline{C}H_2CH_3$), 112.23, 114.25 (2C), 120.51, 120.78, 123.72, 126.54, 127.92 (2C), 128.41 (2C), 130.07, 131.96 (2C), 132.19, 142.43, 142.76, 151.26, 163.43 (arom-C), 144.47 (triazole C_3), 150.61 (triazole C_5), 155.33 (N=CH), 163.70 (COO). UV [Ethanol, λmax, nm (ε, $L.mol^{-1}.cm^{-1}$)]: 312 (17.857), 262 (30.524), 216 (33.305).

Materials

Chemical reagents and solvents were purchased from Aldrich, Fluka, and Merck AG in this research. The melting point was found in the open glass capillary by using a Stuart SMP30 melting point. The ALPHA-P BRUKER FT-IR spectrometer was utilized to obtain IR spectra. ^{1}H and ^{13}C NMR spectrums were registered using Varian spectrometers at 400 MHz and 100 MHz in deuterated dimethyl sulfoxide with the TMS as the internal standard. UV spectra were assessed through a PG Instruments Ltd T80 UV/Vis spectrometer for 10 mm quartz cells between 200 and 400 nm. The coefficients of extinction in $L \cdot mol^{-1} \bullet cm^{-1}$ were explained.

Antioxidant activity

With the aim of evaluating the antioxidant properties of newly synthesized EPM, different antioxidant tests, including free radical scavenging, reducing power, and metal chelating activity, were utilized. According to the method of Oyaizu, reducing potential of EPM can be determined as follows: It could be measured by the degree of conversion of the Fe^{3+}/ferricyanide complex to the Fe^{2+}/ferrous form [25]. At 700 nm, high absorbance demonstrated high reducing potential. The approach on free radical scavenging activity of EPM and standard antioxidants (i.e., butylated hydroxytoluene (BHT), butylated hydroxyanisole (BHA), and α-tocopherol) taken in this study was a methodology based on the method of Blois [26]. Blois defined it as a method in which the reduction capability of DPPH (2,2-diphenyl-1-picrylhydrazyl) radicals was determined by a decrease in its absorbance induced by antioxidants at 517 nm [26]. The decrease in radical absorption of DPPH was due to antioxidants in the reaction of the antioxidant molecule and radical that resulted in scavenging through donation of hydrogen [27]. This was realized to be from purple to yellow as a discoloration. The chelation of ferrous ions by Dinis reported that in quantitative terms, the ferrous ion could form Fe^{2+} complexes [28]. Dinis method was used to estimate the chelation activities of ferrous ions of EPM and standards. In the presence of chelating agents, the complex formation was disrupted, which resulted from the fact that the color of the complex decreased. The complex formation was disturbed by chelating agents, which reduced red color of the complex. Thus, measuring the color decrease in its absorption at 517 nm made it possible to estimate co-existing chelator activities [29].

Quantum chemical calculations

The Gaussian 09 W program was used to carry out all quantum chemical calculations, and the output data were viewed with the GaussView 5.0 software [30, 31]. In DFT method, Becke's three-parameter hybrids function combining with the Lee–Yang–Parr correlation function (B3LYP) [32, 33] foresees the best outcomes for large molecular geometry and vibration frequencies. All the calculations on the computer were carried out by using the B3LYP method and 6–311++G(d,p) level. Calculation of vibrational frequencies, thermodynamic parameters, Mulliken atomic charges, and molecular characteristics were conducted via optimized structural parameters. This detailed vibrational analysis of EPM showed that no negative vibrational assignments represented the optimized molecular structure's stability. To achieve

coherence with the observed frequencies, the computed frequencies were scaled with 0.958 ranging from 1700 to 4000 cm^{-1} and scaled with 0.983 lower than 1700 cm^{-1} B3LYP/6–311++G(d,p) level [34, 35]. Meanwhile, the assignments of specific vibrational modes of EPM were conducted through use of the VEDA 4 Software based upon an analysis of total energy distribution (TED) [36]. The ^{1}H and ^{13}C NMR isotropic chemical shifts were calculated via the GIAO method detailed for EPM, using B3LYP/6–311++G(d,p) level with the IEFPCM method in CCl_4, $CHCl_3$, and DMSO solvents [37]. Additionally, thermodynamic properties (i.e., the entropy, heat capacity, and enthalpy) of EPM at various temperatures (100–1000 ^{o}K) were measured in the gas phase. The electronic behaviors of EPM, oscillator strengths, absorption maximum wavelengths, and excitation energies were found via the B3LYP method of the time-dependent DFT (TD-DFT), on the basis of the optimized structure in the gas phases. The HOMO-1, HOMO, LUMO, and LUMO+1 energy values, energy gaps, and orbital shapes in 3-dimension of EPM were determined and mapped at the same level. The last set of calculations examined the dipole moment, Mulliken atomic charges, and nonlinear optical (NLO) (i.e., linear polarizabilities and first hyperpolarizabilities) at the level mentioned above.

Results and discussion

The Synthesis and Spectroscopic Properties of Compound 4

The synthesis route of EPM for this study was displayed in Scheme 1. 2-Ethoxy-4-formylphenyl-4-methoxybenzoate (1) was synthesized from refluxing 3-ethoxy-4-hydroxybenzaldehyde with 4-methoxybenzoyl chloride with the use of trimethylamine. Following that, the Schiff base, 2-ethoxy-4-[(5-oxo-3-phenyl-1,5-dihydro-1,2,4-triazol-4-ylimino)-methyl]-phenyl-4-methoxybenzoate (EPM) were carried out refluxing 3-phenyl-4-amino-4,5-dihydro-1*H*-1,2,4-triazol-5-one **3** with 2-ethoxy-4-formylphenyl-4-methoxybenzoate **1** in ethanol in the presence of a catalytic amount of acetic acid. The planned product was obtained as colorless crystalline materials with a quite high yield. The structure of this compound was supported through FT-IR, ^{1}H NMR, ^{13}C NMR, and UV–Vis spectroscopic data. In the present study, the recorded band at 3160 in FT-IR for the EPM mentioned above could be attributed to the N–H stretching band. Furthermore, the NH proton signal for EPM was found to be 12.42 ppm. The C=O band was found at 1687 cm^{-1}, while the C=N stretching band was observed at 1610 cm^{-1}. The N=CH proton signal was recorded at 9.68 ppm in ^{1}H-NMR spectra, while the N=CH carbon signal in the ^{13}C-NMR spectra was registered at 155.33 ppm.

Antioxidant activity

To understand the antioxidant activity by considering EPM and the reducing activity of the title compound, standard antioxidants (i.e., BHT, BHA, and α–tocopherol) through use of potassium ferricyanide method were provided. Fe^{3+}–Fe^{2+} transformation was investigated in the synthesized EPM for the evaluation of the reductive capability. The absorbance of EPM in this analysis was lower than that of standard antioxidants. Consequently, no activities were found to reduce complexes of metal ions to their lower oxidation state or to do any electron transfers.

The capacity of hydrogen atoms or electrons donation for EPM and standard antioxidants, including BHA, BHT, and α–tocopherol, was determined through the DPPH. In this respect, the results revealed that the newly synthesized EPM did not report a successful activity as a radical scavenger and did not have any hydrogen donor activity. The ferrous ion chelating activities of EPM and standards, on the other hand, are depicted in Fig. 1. The findings show that EPM exhibited a pronounced iron-binding potential, proposing that their function as peroxidation protectors could be linked to their iron-binding capability. The metal chelating activity of EPM and standards was observed to decrease in the order of EDTA > EPM > α-tocopherol, which were 85.7%, 53.2%, 39.0%, at the lowest concentration, respectively.

Molecular geometry

Figure 2 reveals that the molecular structure optimized with B3LYP/6–311++G(d,p) level. The geometric results obtained from the optimized molecular structure of EPM are presented in Table S1 (Supplementary materials). The data in this table which show the optimized EPM geometric parameters (i.e., torsion angles, bond angles, and bond lengths) were compared with the experimental data [38–40].

The minimum energy value of B3LYP/6–311++G(d,p) level for EPM was recorded as -1561.4231263 Hartree. The distances between the aromatic C–C bonds changed, ranging from 1.390 to 1.405 Å for B3LYP/6–311++G(d,p) level, which was in agreement with those in the molecular structure of EPM due to 1.398–1.377 Å [38]. The N=C bond length in the 1,2,4-triazole ring was recorded as 1.309 Å [38], and the computed N=C (N3=C1) bond length was found to be 1.303 Å. The results showed that the computed N=C bond lengths were slightly larger (0.006 Å) than the experimental values. The length of the C=O bond in the triazole ring recorded as 1.217 Å was compared with the theoretical one; the result displayed that the C=O (C2=O7) was somewhat larger (0.001 Å) than the experimental values [38,

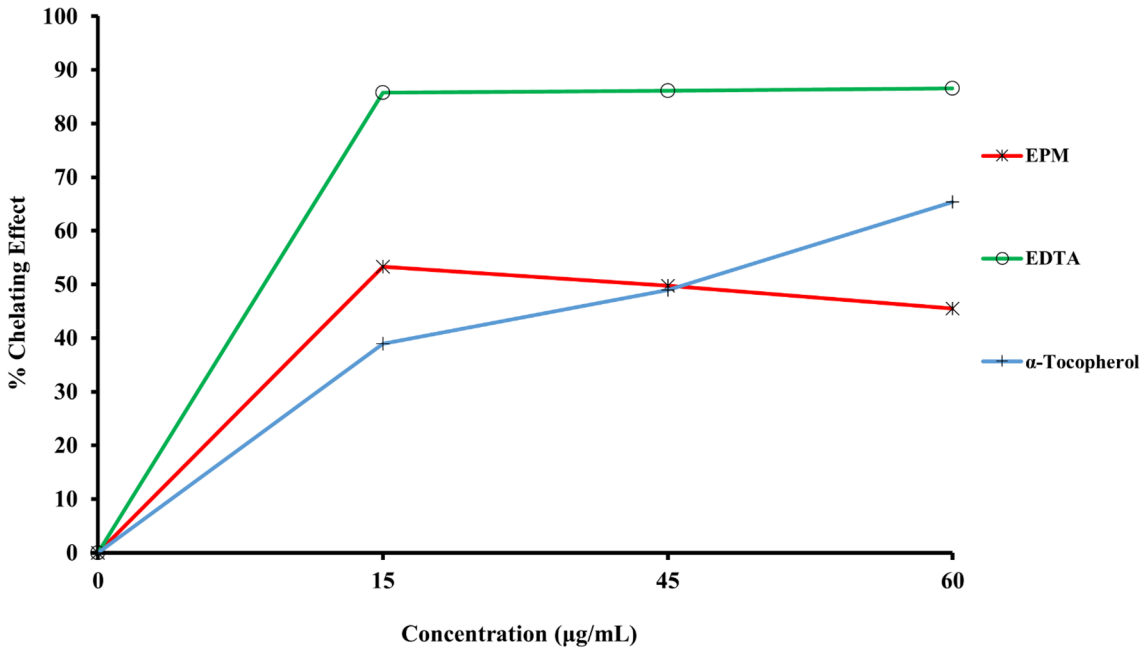

Fig. 1 Metal chelating effect of different amount of 2-ethoxy-4-[(5-oxo-3-phenyl-1,5-dihydro-1,2,4-triazol-4-ylimino)-methyl]-phenyl-4-methoxybenzoate (EPM), EDTA and α-tocopherol on ferrous ions

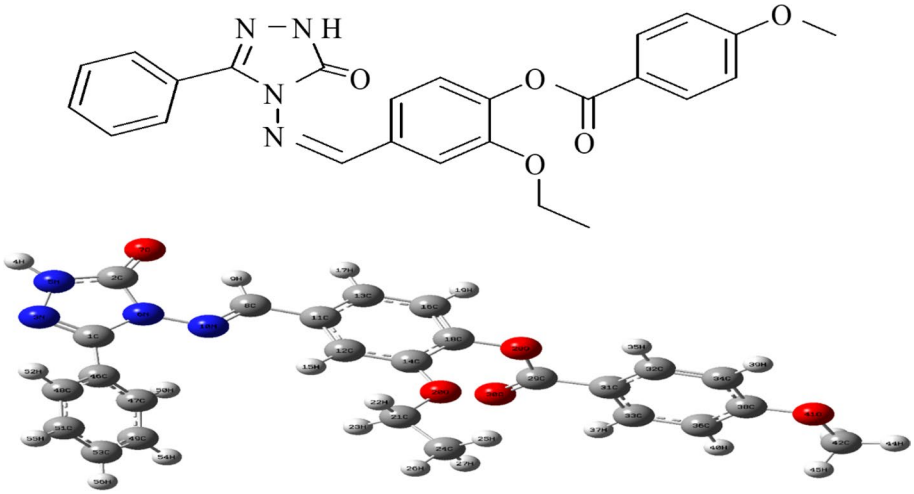

Fig. 2 The chemical structure (top) and optimized molecular structure (bottom) of 2-ethoxy-4-[(5-oxo-3-phenyl-1,5-dihydro-1,2,4-triazol-4-ylimino)-methyl]-phenyl-4-methoxybenzoate with DFT/B3LYP/6–311++G(d,p) level

40]. The optimized C–O bond lengths were calculated to be 1.424 (C42–O41) and 1.434 (C21–O20), the bond lengths of the C–O in the aliphatic group were larger than the experimental ones (1.481 Å) because the electron density was more localized on methoxy and ethoxy groups. Additionally, the N6–C1 bond length was discovered to be 1.470 Å which was higher because of the conjugation to the phenyl ring and the contribution provided by its electronegativity character as can be seen in Table S1 (Supplementary materials). The basic differences in the length of the C-H bond could be determined by inductive and mesomeric interactions, as well as the electric dipole of the polar substituents. The scan of the potential energy surface of EPM was performed for the evaluation of the stable conformation. It can be noted that the bond H–C–H angles of the methyl groups were nearly equivalent to 109°. Nearly every bond C–C–C angles in the ring were − 120°. The O-C-H angles at 6–311++G(d,p) level seemed to be 109.5°. Each of the above-mentioned structural parameters confirmed that O-CH_3 and O–CH_2CH_3 groups in benzene rings were slightly out of the standard hexagonal structure. For conformation flexibility, the internal redundant coordinative dihedral angle D (N10–C8–C11–C12) was selected in the PES scan. The geometric parameters were relaxed through scanning, while the torsional angle of

D (N10–C8–C11–C12) changed by 10 degrees from 0° to 360° degrees. The potential surface energy scan graph and optimized structure for EPM can be seen in Fig. 3. As shown in Fig. 3, the C8-C11 bond axis of the N10–C8–C11–C12 dihedral angle was located between 4,5-dihydro-1,2,4-triazol-5-one and phenyl rings. The energy value of the C3 conformer was computed at B3LYP/6–311++G(d,p) level, showing a minimum energy value of −1561.424 Hartree and the most stable state for EPM. Besides that, the second stable form of C1 was found with an energy of −1561.423 Hartree. However, the C2 conformer was the most unstable, with an energy value of −1561.412 Hartree for the compound mentioned above. Two minimum saddle points (~250° and 450°) were also obtainable.

These results are consistent with those of experimental studies and only slight differences were observed between experimental and theoretical results because the computed results belong to the isolated molecule in the gaseous phase and the experimental results belong to the molecule in the solid-state [38, 40]. The findings of this study backed up the findings of many previous studies in this field.

IR spectrum

Vibrational analysis

This study probed to obtain data that would help in addressing these spectroscopic analyses of EPM. The B3LYP/6–311++G(d,p) level was used to calculate theoretical vibration modes. EPM consisted of 56 atoms and 162 normal vibration modes. Thus, it was distributed to 162 normal vibration modes, taking the symmetry of the C1 point group into consideration, as in the following;

$$\Gamma_{vib} = 109A' + 53A''$$

Based on C1 symmetry, the distribution of 162 fundamental vibrations belonging to the molecule could be made as 109 in-plane vibrations of A′ species and 53 out-of-plane vibrations of A″ species. Regarding B3LYP/6-311++G(d,p) basis set, the factors of scaling fact were 0.958 and 0.983. IR spectra were active vibrations of EPM under C1 symmetry. The observed and calculated vibrational frequency modes, IR intensities, and Raman scattering activities for EPM are presented in Table 1. In this context, the C1, C2, and C3 conformers' vibrational frequency modes were calculated, and one imaginary frequency of the C2 conformer was found. The result indicates that the conformer C2 was in an unstable transition state. The data presented in Table 1 reveal that no imaginary value was observed for C3 conformer. In comparison, this conformation's computed frequency values were very similar to that of the stable C1 conformer.

Moreover, the experimental and simulated IR spectrums at the B3LYP/6–311++G(d,p) level of EPM are presented in Fig. 4. When the experimental and calculated results were compared, it can be seen that these vibrational values

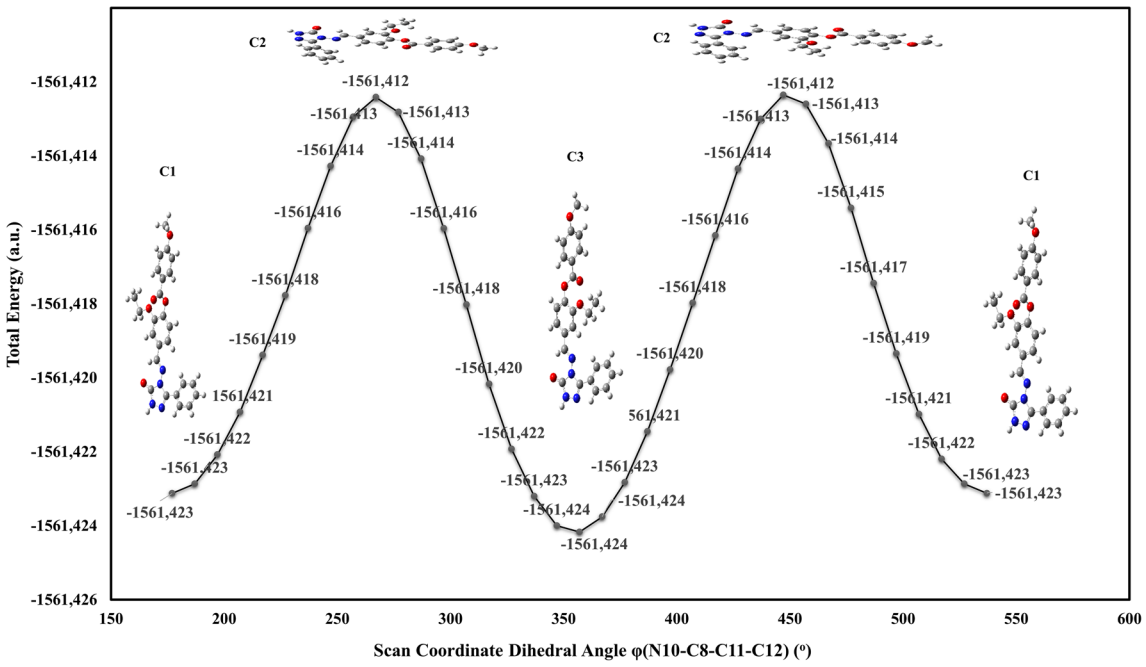

Fig. 3 The scanned potential energy surface with DFT/B3LYP/6–311++G(d,p) level of 2-ethoxy-4-[(5-oxo-3-phenyl-1,5-dihydro-1,2,4-triazol-4-ylimino)-methyl]-phenyl-4-methoxybenzoate

Table 1 Experimental and calculated (unscaled and scaled) B3LYP/6–311++G(d,p) level vibrational frequencies (cm^{-1}), IR intensity (km mol^{-1}), Raman intensity, force constant (mdyne $Å^{-1}$), and probable assignments of 2-ethoxy-4-[(5-oxo-3-phenyl-1,5-dihydro-1,2,4-triazol-4-ylimino)-methyl]-phenyl-4-methoxybenzoate

Experimental frequencies		B3LYP 6–311++G(d.p)				Characterization of normal modes with PED (%)
	FT-IR	Unscaled	Scaled	IR intensity I_{IR}	Raman intensity S_{Raman}	
1	–	12.22	12.07	0.6	1.38	$\tau CCCN\ (24)_{imine} + \tau C_8N_{10}N_6C_1$ (37) in triazole
2	–	14.63	14.45	0.3	2.76	$\tau C_{31}C_{29}O_{28}C_{18}$ (59)
3	–	18.65	18.43	0.31	1.6	$\tau C_{11}C_8N_{10}N_6$ (12) + $\tau O_{28}C_{18}C_{16}C_{13}$ (27) + $\tau C_{13}C_{11}C_8N_{10}$ (12)
4	–	30.10	29.74	0.16	6.59	[τOCCC (19) + τCCOC (13)] in rings
5	–	31.48	31.10	0.12	1.65	$\delta N_6C_1C_{46}$ (10) + [τCCCO (12) + τOCCC (11)] in rings
6	–	42.87	42.36	0.61	4.63	$\tau C_2N_5N_3C_1$ (32) in triazole
7	–	53.17	52.53	1.53	1.47	[τCCCO (25) + τCC_1OC (14) + τCOCC (12)] in rings
8	–	61.67	60.93	0.79	1.88	[τCNNC (15) + τNNCN (10)] in triazole
9	–	69.81	68.97	0.06	4.31	[τOCCC (12) + τCCOC (30)] in rings
10	–	77.26	76.33	1.38	0.83	[τNNCN (16) + γNNCC (12)] in triazole + γCCCC (13) in rings
11	–	84.70	83.68	0.09	0.32	[τCCCO (10) + τCOCC (26)] in rings
12	–	89.59	88.51	0.16	1.48	[δNCC (12) + τCNNC (16)] in triazole
13	–	99.85	98.65	1.11	0.76	[τCCOC (12) + τCOCC (55)] in rings
14	–	112.93	111.57	1.55	0.57	$\delta C_{31}C_{29}O_{28}$ (13)
15	–	126.14	124.63	2.92	1.66	τCNNC (11) in triazole + τCOCC (16) in rings
16	–	129.55	128.00	4.89	1.69	τCOCC (23) in rings
17	–	145.54	143.79	0.65	0.63	$\delta C_{21}O_{20}C_{14}$ (15)
18	–	152.35	150.52	5.14	1.78	$\tau C_{13}C_{11}C_8N_{10}$ (20)
19	–	205.56	203.09	1.21	2.28	$\tau CCCN\ (10) + \tau C_2N_5N_3C_1$ (13) in triazole
20	–	207.80	205.31	8.22	1.88	δOCC (11) in rings + $\tau C_{13}C_{11}C_8N_{10}$ (12)
21	–	218.01	215.39	1.01	1.91	[δOCC(11) + δCCC (12)] in rings
22	–	227.24	224.51	0.66	1.42	τHCOC (50) in rings
23	–	232.11	229.32	2.35	0.48	τHCOC (23) in rings
24	–	243.48	240.56	1.45	1.3	τHCOC (13) in rings
25	–	257.35	254.26	0.2	0.45	[τHCOC (48) + τH_7CCO (13)] in rings
26	–	291.48	287.98	7.46	3.59	τHCOC (20) in rings
27	–	304.46	300.81	3.08	2.07	τCCCC (11) in rings
28	–	313.80	310.03	0.86	1.71	τCCCC (10) in rings
29	–	320.31	316.47	2.53	0.1	τCCCC (10) in rings
30	–	330.31	326.35	0.15	10.45	τCCCC (13) in rings
31	–	333.33	329.33	8.67	0.78	[δOCO (11) + δOCC (11) + τCCCC (10)] in rings
32	–	354.71	350.45	1.34	0.66	[τOCCC (10) + τCCOC(23)] in rings
33	–	391.95	387.25	8.94	1.18	δOCN (10) in triazole + δCCC (12) in rings
34	–	409.29	404.38	4.04	3.11	$\tau C_{11}C_8N_{10}N_6$ (15)
35	–	412.43	407.48	1.46	1.74	τCCCC (70) in rings
36	–	420.81	415.76	21.3	1.4	$\delta O_7C_2N_5$ (17) + $\delta N_3C_1N_6$ (15) in triazole
37	–	427.89	422.76	0.43	0.38	τHCCC (15) + τCCCC (34) + τCCCO (27) in rings
38	–	429.14	423.99	9.6	4.68	$\tau C_{14}C_{12}C_{11}C_{13}$ (18) in rings
39	432 m	469.49	463.86	72.57	1.27	$\tau H_4N_5N_3C_1$ (46)
40	–	477.07	471.35	3.87	0.67	[τHCCC (12) + τCCCC (36) + γOCCC (15)] in rings
41	–	514.04	507.87	5.78	0.99	[τHCCC (17) + γOCCC] in rings
42	–	516.38	510.18	10.32	2.32	δOCC (11) + δCOC (14)
43	–	516.98	510.78	7.94	3.53	$\delta O_{41}C_{38}C_{36}$ (11) + $\delta C_{42}O_{41}C_{38}$ (14)
44	–	559.28	552.57	0.82	2.42	$\delta O_{20}C_{14}C_{12}$ (30) + $\delta C_{31}C_{29}O_{28}$ (12)
45	–	575.97	569.06	3.98	1.14	$\delta O_{20}C_{14}C_{12}$ (18)

Table 1 (continued)

Experimental frequencies		B3LYP 6–311++G(d.p)				Characterization of normal modes with PED (%)
	FT-IR	Unscaled	Scaled	IR intensity I_{IR}	Raman intensity S_{Raman}	
46	–	610.60	603.27	5.54	6.59	δCCC (14) in rings
47	–	623.35	615.87	47.89	1.62	$\gamma O_{20}C_{12}C_{18}C_{14}$ (14)
48	614 m	630.20	622.64	7.79	3.56	$\delta O_7C_2N_5$ (14) in triazole + δCCC (29) in rings
49	–	634.63	627.01	7.61	7.42	$\delta O_7C_2N_5$ (14) in triazole + δCCC (26) in rings
50	–	639.03	631.36	17.62	5.47	[$\gamma O_{20}C_{12}C_{18}C_{14}$ (15) + γCCCC (13)] in rings
51	–	646.30	638.54	15.58	11.52	[νCC (22) + δCCC (34) + δOCC (13)] in triazole
52	–	682.27	674.08	21.94	7.37	δCCC (41) in rings
53	688 m	701.97	693.55	21.35	1.43	[τCCCO (25) + γOCOC (19)] in rings
54	–	702.53	694.10	50.5	0.26	τHCCC (24) in rings + [τNNCN (10) + γNNCC (20)] in triazole
55	–	705.26	696.80	20.37	0.18	τHCCC (29) in rings + $\tau C_{13}C_{11}C_8N_{10}$ (15)
56	–	728.98	720.23	4.88	12.94	[τHCCC (17) + τCCCC (23)] in rings + $\gamma O_{20}C_{12}C_{18}C_{14}$ (15)
57	725 s	738.26	729.40	16.99	2.14	γONNC (73) in triazole
58	–	750.03	741.03	24.95	4.21	γONNC (32) in triazole
59	761 w	775.32	766.02	29.61	1.76	τCCCO (10) + γOCOC (10) + γOCCC (10)
60	–	783.05	773.65	30.66	2.04	τHCCC (35) in rings
61	–	797.61	788.04	10.74	36.89	νCC (18) in rings + $\nu O_{41}C_{38}$ (12)
62	797 s	805.06	795.40	25.25	12.58	[νNC (16) + δCNN (31)] in triazole
63	–	819.05	809.22	1.75	27.19	$\nu O_{20}C_{14}$ (12) + τHCCC (29) in rings
64	–	826.53	816.61	1.03	0.57	τHCCC (90) in rings
65	–	832.86	822.87	3.91	0.71	$\tau H_{22}C_{21}O_{20}C_{14}$ (75)
66	–	837.62	827.57	1.07	8.45	νCC (15) in rings
67	–	852.90	842.67	13.31	3.18	[νNN (10) + δNCN (21) + δCCN (19)] in triazole
68	–	855.67	845.40	2.2	1.66	τHCCC (53) in rings
69	851 s	860.73	850.40	34.38	0.06	γOCCC (46) + τHCCC (46) in rings
70	–	867.00	856.60	9.71	0.24	τHCCC (55) in rings
71	–	882.95	872.35	21.7	41.78	$\delta O_{30}C_{29}O_{28}$ (11) + τHCCC (15) in rings
72	–	910.01	899.09	10.37	1.94	νCC (13) + $\nu O_{20}C_{21}$ (20) in rings
73	–	939.34	928.07	11.91	0.19	τHCCC (57) in rings
74	–	967.08	955.48	52.26	14.01	$\delta N_5N_3C_1$ (30) in triazole
75	958 m	971.74	960.08	5.14	0.65	τHCCC (64) in rings
76	–	977.75	966.02	0.57	0.13	τHCCC (73) + τCCCO (10) in rings
77	–	989.96	978.08	1.5	0.2	τHCCC (60) in rings
78	–	990.32	978.44	0.23	0.04	[τHCCC (80) + τCCCC (13)] in rings
79	–	996.08	984.13	33.81	13.04	νCC (14) in rings
80	–	1004.03	991.98	0.27	0.64	[τHCCC (62) + τCCCC (27)] in rings
81	1024 s	1009.61	997.49	14.92	10.26	$\tau H_9C_8N_{10}N_6$ (85)
82	–	1016.83	1004.63	0.59	69.78	[νCC (33) + δCCC (34)] in rings
83	–	1021.76	1009.50	59.3	1.84	[δCCC (64) + δHCC (11)] in rings
84	1045 s	1050.85	1038.24	6.99	26.49	[νCC (36) + δCCC(16) + δHCC (16)] in rings
85	–	1052.56	1039.93	207.9	8.84	$\nu O_{41}C_{42}$ (62)
86	–	1058.75	1046.05	70.8	4.52	$\nu O_{20}C_{21}$ (35) + νCC (30) in rings
87	1075 vs	1070.39	1057.55	355.91	50.04	$\nu O_{20}C_{14}$ (31) + $\delta O_{30}C_{29}O_{28}$ (10)
88	–	1095.37	1082.23	17.75	21.5	νCC (13) in rings + νN_5N_3 (37)
89	1120 s	1112.46	1099.11	7.84	24.7	[νCC(11) + δHCC (10)] in rings + νN_5N_3 (14)
90	–	1129.12	1115.57	68.58	150.59	[νCC (10) + δHCC (24)] in rings
91	–	1134.54	1120.93	11.69	1.85	[νCC (10) + δHCC (62)] in rings
92	–	1140.11	1126.43	155.54	117.34	$\nu O_{20}C_{21}$ (11) + [δHCC (11) + δHCCO (12)] in rings

Table 1 (continued)

Experimental frequencies		B3LYP 6–311++G(d.p)				Characterization of normal modes with PED (%)
	FT-IR	Unscaled	Scaled	IR intensity I_{IR}	Raman intensity S_{Raman}	
93	–	1152.58	1138.75	12.93	205.55	[νN_5C_2 (11) + $\delta N_3C_1N_6$ (11)] in triazole + δCCC (10) in rings
94	1162 s	1167.55	1153.54	0.76	2.64	δHCH (24) + $\tau H_{43}C_{42}O_{41}C_{38}$ (75)
95	–	1177.11	1162.98	4.21	2.44	δHCO (41) + τHCOC (38) + τHCCO (11)
96	1195 s	1180.05	1165.89	411.74	496.55	νOC (11) + δHCC (40) in rings
97	–	1184.00	1169.79	0.07	6.41	[νCC (13) + δHCC (71)] in rings
98	–	1187.44	1173.19	141.18	87.04	δHCC (35) in rings
99	–	1202.03	1187.61	18.41	3.74	δHCH (22) in rings + τHCOC (54)
100	–	1206.84	1192.36	8.89	5.14	δHCC (41) in rings
101	–	1211.40	1196.86	114.26	8.49	νN_5C_2 (12) in triazole + $\nu O_{20}C_{14}$ (20)
102	–	1228.44	1213.70	183.88	40.53	δHCC (14) in rings
103	–	1269.17	1253.94	766.68	462.12	νCC (30) in rings
104	1260 vs	1285.42	1269.99	115.31	4.64	νOC (43) + δHCC (13)
105	–	1290.76	1275.27	112.79	215.23	δHCC (26) in rings
106	–	1296.07	1280.52	54.11	329.55	νN_5N_3 (17) in triazole
107	–	1305.79	1290.12	2.07	7.97	δHCO (53) + τHCOC (26)
108	–	1315.76	1299.97	346.76	119.52	νCC (10) + δHCC (17) in rings
109	–	1326.31	1310.39	6.58	3.46	νCC (50) in rings
110	–	1327.05	1311.13	3.98	1.64	δHCC (82)in rings
111	–	1346.28	1330.12	49.76	451.25	νCC (53) in rings
112	–	1351.81	1335.59	66.78	16.71	νCC (22) in rings
113	1358 s	1356.20	1339.93	9.74	12.83	[νCC (11) + δHCC (36)] in rings
114	1394 m	1379.30	1362.75	196.45	0.45	[νNC(19) + δHNN (13)] in triazole + δHCN_{imine}(27)
115	–	1401.77	1384.95	3.46	9.31	δHCH (51) + τHCOC (25)
116	1429 s	1403.98	1387.13	17.2	62.28	δHNN(42) in triazole + δHCN_{imine} (12)
117	–	1427.16	1410.03	41.7	9.63	δHCH (32) in rings + τHCOC (36)
118	–	1430.60	1413.43	55.47	38.91	τHCOC (23)
119	1448 s	1448.72	1431.34	0.87	0.73	νCC (41) + δHCC (30) in rings
120	–	1457.98	1440.48	107.25	39.65	δHCN_{imine} (22)
121	–	1476.53	1458.81	6.16	5.68	δHCH (85) in rings
122	–	1477.84	1460.11	65.73	43.59	νCC (27) + δHCC (22) in rings
123	–	1484.72	1466.90	8.57	8.88	δHCH (73) + τHCOC (11) in rings
124	–	1494.30	1476.37	9.69	16.35	δHCH (76) + τHCOC (23) in rings
125	–	1501.21	1483.20	6.7	12.14	δHCH (60) + τHCCO(12) in rings
126	–	1503.81	1485.76	42.68	8.7	δHCH (74) + τHCOC (22) in rings
127	–	1520.06	1501.82	25.88	2.17	δHCH (77) in rings
128	1510 s	1528.18	1509.84	35.04	4.72	δHCC (25) in rings
129	–	1539.33	1520.86	23.16	13.19	δHCC (39) in rings
130	1541 s	1544.00	1525.47	151.82	32.52	δHCC (36) in rings
131	–	1593.35	1574.23	32.7	217.15	νN_3C_1 (42) in triazole + νCC (12) in rings
132	1581 s	1609.29	1589.98	5.1	31.29	νCC (33) + δCCC (11) in rings
133	–	1612.51	1593.16	58.74	2062.94	νCC (26) + δCCC (11) in rings
134	–	1626.14	1606.63	27.11	79.53	νCC (35) + δCCC (13) in rings
135	–	1635.80	1616.17	53.51	1170.86	νCC (54) + δHCC (11) in rings
136	–	1644.65	1624.91	0.16	307.05	[νCC (40) + $\delta H_{35}C_{32}C_{34}$ (29)] in rings
137	–	1645.46	1625.71	270.19	269.11	$\nu C_{14}C_{12}$ (45) in rings
138	1610 s	1657.21	1637.32	9.82	1656.59	νN_3C_1 (59) in triazole
139	1687 vs	1782.26	1760.87	566.24	16.27	[νO_7C_2 (73) + νN_5C_2 (12)] in triazole

Table 1 (continued)

Experimental frequencies		B3LYP 6–311++G(d.p)				Characterization of normal modes with PED (%)
	FT-IR	Unscaled	Scaled	IR intensity I_{IR}	Raman intensity S_{Raman}	
140	1732 vs	1786.94	1765.50	293.14	325.49	νOC (87)
141	–	3003.26	2883.13	33.19	89.74	νCH_2 (78)
142	2850 w	3011.82	2891.35	60.38	191.15	νCH_3 (99)
143	–	3039.00	2917.44	19.72	190.99	νCH_2 (71) + νCH_3 (27)
144	2883 w	3042.47	2920.77	21.27	53	νCH_2 (96)
145	–	3073.65	2950.70	31.75	63.48	νCH_3 (100)
146	2922 w	3105.85	2981.62	23.18	81.84	νCH_2 (87) + νCH_3 (10)
147	–	3115.75	2991.12	22.34	38.19	νCH_2 (39) + νCH_3 (60)
148	2973 w	3139.51	3013.93	21.09	166.25	νCH (99) in rings
149	–	3153.27	3027.14	0.95	18.77	νCH (100) in rings
150	–	3165.22	3038.61	0.02	50.09	νCH(100) in rings
151	–	3176.17	3049.12	11.46	121.33	νCH (99) in rings
152	–	3187.40	3059.90	19.09	182.71	νCH (92) in rings
153	–	3188.49	3060.95	4.76	60.29	νCH (93) in rings
154	–	3190.88	3063.24	4.46	55.16	νCH (95) in rings
155	–	3193.47	3065.73	0.14	72.9	νCH (100) in rings
156	–	3199.34	3071.37	3.47	51.54	νCH (99) in rings
157	–	3200.83	3072.80	5.77	143.41	νCH (92) in rings
158	–	3208.72	3080.37	1.3	98.69	νCH (83) in rings
159	–	3209.76	3081.37	9.21	72.07	νCH (100) in rings
160	–	3212.35	3083.86	1.6	162.15	νCH (94) in rings
161	3056 m	3219.36	3090.59	2.03	108.9	νCH (98) in rings
162	3160 m	3673.90	3526.94	134.03	276.99	νNH (100) in triazole
RMSD			**56.30**			

ν stretching, δ bending, γ out-of-plane bending, τ torsion, *s* strong, *m* medium, *w* weak, *v* very, IR intensities (km/mol), S_R Raman scattering activities ($Å^4$/amu), *RMSD* Root Mean Square Deviation

differed slightly from each other. As can be seen in the table (above), the computed IR data were significantly higher than the experimental ones. The explanation of the observed correlation for theoretical and experimental data could be made in this way. The most likely reasons can be suggested as follows; first theoretical DFT calculations may have verified experimental results which were specific for the vibrational study. Moreover, they might usually be restricted to simple harmonic method, supplying a characterization that needed a scaling factor to achieve vibrational frequencies. The computed data were also acquired in the isolated vacuum state, but experimental data were obtained in solid form. The scaled and unscaled theoretical frequencies, potential energy distributions (PED), Raman activities, and IR intensities, together with assignments for EPM, are displayed in Table 1. The computed and experimental values showed a good correlation with each other (Fig. S1) (Supplementary materials).

$$\upsilon_{calc} = 1.0485\upsilon_{exp} - 55.299\left(R^2 = 0.9951\right)$$

N–H vibrations

In the present case, the study's compound was a heterocyclic aromatic system in 1,2,4-triazole ring fused. For secondary aromatic amines, medium-intensity bands were characterized in solid and liquid phases at 3400–3000 cm^{-1} [41]. The absorption position in this region depended on the degree of hydrogen bonding and the physical condition of the sample or solvent polarity. The medium-intensity band observed at 3160 cm^{-1} was assigned to the N–H stretching vibration band in the current study. The N–H stretching band at 3526.94 cm^{-1} in FT-IR was in good agreement with B3LYP/6–311++G(d,p) values. The N–H scissoring vibrational band occurs typically in the region 1580–1650 cm^{-1} [41]. In the present study, this

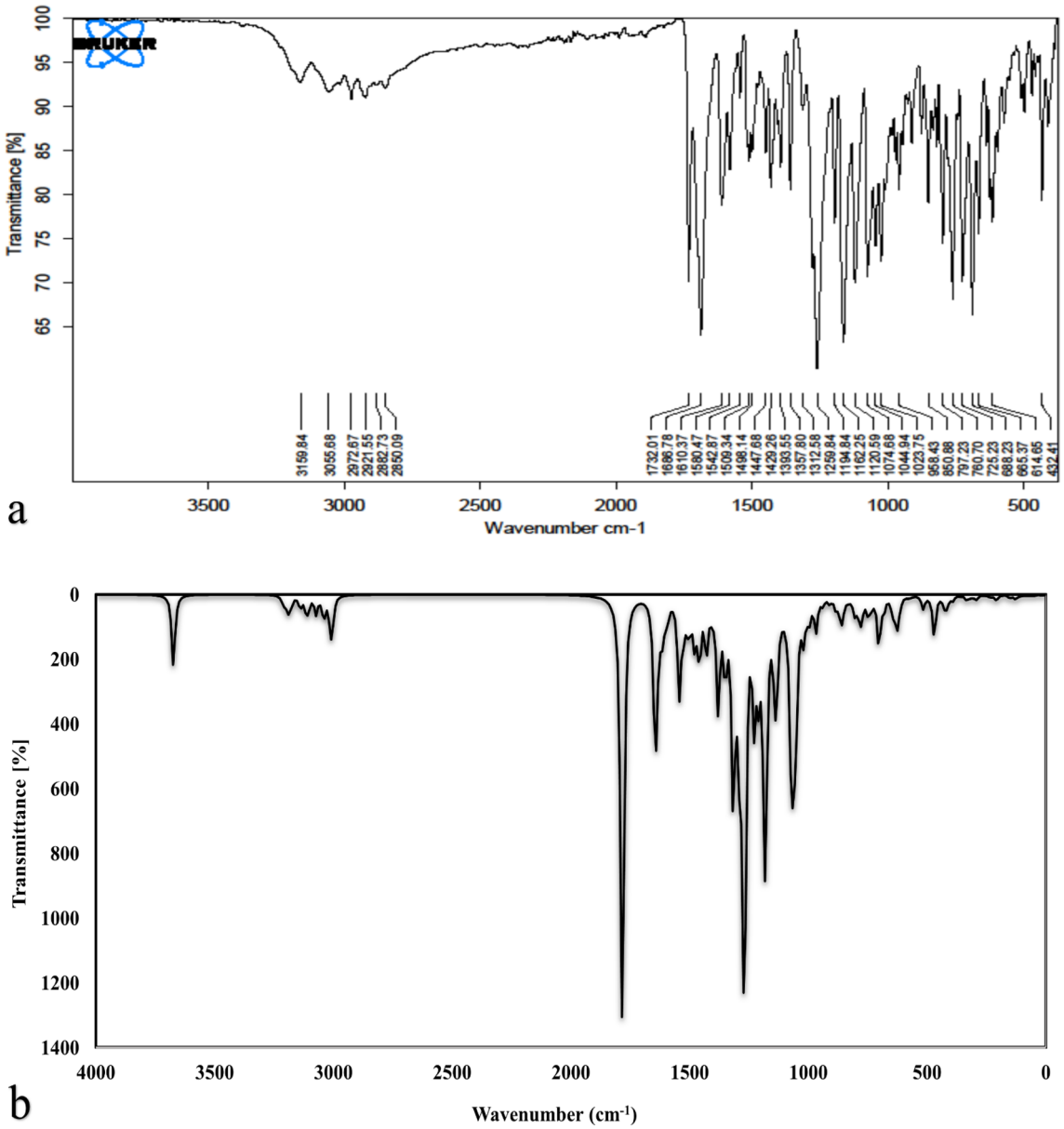

Fig. 4 IR spectra (**a**) experimental and (**b**) simulated with DFT/B3LYP/6–311++G(d,p) level of 2-ethoxy-4-[(5-oxo-3-phenyl-1,5-dihydro-1,2,4-triazol-4-ylimino)-methyl]-phenyl-4-methoxybenzoate

vibrational band for EPM was found as a strong-intensity band at 1610 cm^{-1}. The theoretically scaled N–H scissoring vibrational band was identified at 1637.32 cm^{-1}, and it altogether correlated with the experimental value. As expected, this mode was purely stretching mode as the PED column showed that the mode was 96%. The wagging and twisting modes of the N–H group were therefore assigned to the vibrational bands at 614 and 432 cm^{-1}, respectively. The theoretically scaled N–H wagging and twisting modes were identified at 622.64 and 463.86 cm^{-1}, respectively. As could be seen from the table above, the findings were identical to those found in triazole. The computed and experimental values showed a good correlation with each other.

C-H vibrations

In aromatic compounds, the C-H stretching vibrational modes were generally identified in the region 3000–3100 cm^{-1} [41–44]. In addition, the stretching vibrational modes for the aliphatic C-H group were observed in the region 2950-2850 cm^{-1} [41–44]. For EPM, the C-H stretching vibrational modes in IR spectra were noted at 3056 cm^{-1}. The theoretically scaled C-H stretching

vibrational modes in aromatic rings were found at intervals 3100–3250 cm^{-1}.

The aromatic C-H in-plane and out-of-plane bending vibrational modes occurred in 1000–1300 cm^{-1} and 900–667 cm^{-1}, respectively [41, 44], and such vibrational modes were quite informative. These were extremely helpful in characterization of the molecule. Similarly, the noted modes at 1448 cm^{-1} of EPM can be attributed to the C-H in-plane bending vibrational modes combined with other vibrational modes, while the recording modes at 958 cm^{-1} of EPM can be assigned to the C-H out-of-plane bending vibrational modes. The noted modes at 1431.34 cm^{-1} of EPM could be attributed to C-H in-plane bending in conjunction with other vibration bands, whereas the noted modes at 960.08 cm^{-1} could be allocated to the C-H out-of-the planning bending vibrations. The determined wavenumbers and assignments for the C-H stretching, in-plane, and out-of-plane bending modes of EPM are given in Table 1. In comparison, the stretching vibration bands of aliphatic C-H were observed as weak bands at 2973, 2922, 2883, 2850, 2950.70, and 2891.35 cm^{-1}, while the measured mode values at the B3LYP/6–311++G(d,p) level were found to be 3013.93, 2981.62 cm^{-1}, respectively. Additionally, the "strong band" observation at 1385 cm^{-1} was attributed to the in-plane bending vibration mode of EPM, whereas the observation of the "strong band" at 1045 cm^{-1} was assigned to the C-H out-of-plane bending vibration mode of the aliphatic group.

C–C and C=C vibrations

The stretching vibration modes are crucial in the spectrum of benzene and its derivatives, which are characteristics of the aromatic ring. The main C=C ring stretching modes of aromatic compounds were registered at 1620–1390 cm^{-1}. In this area, the C=C stretching modes at 1581,1541, and 1510 cm^{-1}, and the C–C mode at 1448 cm^{-1} were noted, while the computed mode values were found to be 1589.29, 1525.47, and 1509.84 cm^{-1} for C=C stretching modes and 1431.34 cm^{-1} for C–C mode. Some modes were below 700 cm^{-1} for the aromatic ring. These modes are susceptible to changes in the substitution's nature and location. For phenyl rings, vibration modes were observed at 958 and 851 cm^{-1} in IR spectra, and their corresponding computed modes were 960.08 and 850.40 cm^{-1}.

C=O and C–O vibrations

Aldehydes, ketones, acid halides, carboxylic acids, anhydrides, carboxylic esters, amides, lactones, and lactams have an exceptionally strong C=O stretching absorption mode in the area of 1770–1540 cm^{-1} [41, 44]. Within its relevant interval, the C=O stretching mode was affected by external factors such as the physical state of the molecule, ring pressure, the mass and electronic influence of neighboring substituents, conjugation, and hydrogen bonding. Consideration of these variables leads to a substantial amount of knowledge about the environment of the C=O group. The stretching modes of the C=O group typically take place within the range of 1740–1690 cm^{-1}. The experimental C=O stretching mode for EPM was located at 1732 cm^{-1} (IR) in the current study. Its corresponding calculated values were observed to be at 1765.50 and 1760.87 cm^{-1}. The in-plane bending was allocated at 688 cm^{-1}, and their corresponding computed mode was 693.55 cm^{-1}. The C=O vibration modes were consistent with experimental findings. According to previous literature, the C–O stretching modes are to be expected in the wavelength between 1300 and 1000 cm^{-1} [44]. Due to the presence of one $–OCH_3$ and one $–OCH_2CH_3$ groups, the molecule is expected to possess the four C–O stretching, the C–O in-plane bending vibrations, and four C–O out-of-plane bending vibrations. The C–O stretching vibration modes of EPM were recorded to be at 1260, 1195, 1162, and 1075 cm^{-1}. The C-O in-plane-bending vibration modes were computed at 1269.99, 1165.89, 1153.54, and 1057.55 cm^{-1}. The relevant out-of-plane bending vibrations were found to be at 350.45 329.33, 287.98, and 229.32 cm^{-1}.

C–N and C=N vibrations

The C=N stretching mode with medium intensity was located at 1610 and 1687 cm^{-1} in the FT-IR spectrum [43, 44]. The theoretical values of 1760.87 and 1637.32 cm^{-1} were well agreed, consistent with experimental findings. The difficulty of identifying C–N vibrations is that there are many overlapping bands in this area. However, in this study, the C–N stretching vibration modes are recognized and allocated by theoretical calculations. Aromatic amines exhibited strong C-N stretching absorptions in the 1342–1266 cm^{-1} region; in particular, aromatic primary amines showed strong C-N stretching absorptions at approximately 1300 cm^{-1}. The IR spectra measurements of the C-N stretching modes showed that its related modes in the IR spectrum were observed at 1394 and 1024 cm^{-1}. Theoretically, the corresponding bands were measured at 1362.75 and 997.49 cm^{-1}. In addition to this, the infrared absorption at 797 cm^{-1} was definitively assigned to the triazole ring's C-N stretching mode. They were in accordance with the experimental results. As shown in Table 1, the in-plane and out-of-plane vibration modes of C-N were also allocated in their respective region. The findings of this study also endorsed analogous compounds of triazole.

NMR spectral analysis

^{13}C and ^{1}H NMR spectral analysis

Isotropic chemical shift values are often used to help identify both reactive organic and ionic species. It is suggested

that correct molecular geometry predictions are essential in reliable magnetic characteristic calculations. The geometry optimization of EPM was thus performed with B3LYP/6–311++G(d,p) level. Following that, the ^{1}H and ^{13}C chemical shift calculations of the EPM were performed through Gauge-Independent Atomic Orbital (GIAO) method [45]. The hydrogen and carbon shielding tensors of EPM were experimentally and theoretically investigated**.** Chemical shift values for ^{1}H and ^{13}C NMR spectrums (relative to TMS) were recorded in ppm. The experimental $^{13}C/^{1}H$-NMR spectrums are displayed in Fig. 5. The hydrogen and carbon shielding tensors of EPM were evaluated in solvent (DMSO, CCl_4, and $CHCl_3$). The GIAO approach was somewhat better as the calculated characteristics converged quicker when the basis set was used. Because of its significantly reduced computing costs, density functional methodologies offer an efficient alternative to traditional correlating methods. The ^{13}C NMR chemical shifts spectrums for the organic compounds are usually more than 100 (> 100); precision ensures that spectroscopic parameters are interpreted reliably**.** In general, the aromatic carbons were in a 100–170 ppm area. In the current study, however, the aromatic carbon signals of EPM were found at 112.23–163.43 ppm. Theoretically, the corresponding signals were found at intervals 110–175 ppm. The carbon atom signals in 1,2,4 triazole ring for EPM were found at 144.47 and 150.61 ppm. Such signals were computed at 152.34 (gas phase), 152.96 (DMSO), 152.63 (CCl_4), and 152.80 ($CHCl_3$) ppm and 154.98 (gas phase), 155.99 (DMSO), 155.47 (CCl_4), and 155.74 ($CHCl_3$), respectively. Furthermore, there existed an electronegative effect in two oxygen atoms at two distinct places in the molecule; hence, the C14, C18, and C38 chemical shift values appeared to be 151.26, 142.43, and 163.43 ppm, respectively. The relevant signals for C14 were found to be at 157.81 (gas phase), 157.61 (DMSO), 157.83 (CCl_4), and 157.77 ($CHCl_3$) ppm, respectively. The corresponding signals for C18 were observed at 150.26 (gas phase), 149.10 (DMSO), 149.85 (CCl_4), and 149.52 ($CHCl_3$) ppm, respectively. Furthermore, The C38 signals were appeared at 170.44 (gas phase), 171.88 (DMSO), 171.05 (CCl_4), and 171.44 ($CHCl_3$) ppm, respectively. In the methoxy and ethoxy groups, the carbon atoms C21 and C42 were at 64.02 and 55.56 ppm. Its related computed signals were observed to be at 65.91 (gas phase), 66.50 (DMSO), 66.16 (CCl_4), and 66.32 ($CHCl_3$) ppm, and 56.06 (gas phase), 56.78 (DMSO), 56.35 (CCl_4), and 55.56 ($CHCl_3$) ppm respectively. The C24 carbon atom was allocated to the signal found at 14.32 ppm, while the recorded signal at 15.02 (the gas phase), 14.93 (DMSO), 14.94 (CCl_4), and 14.92 ($CHCl_3$) ppm could be assigned. A linear regression curve was drawn for the EPM molecule and displayed in Fig. S2 (Supplementary materials). The regression coefficients for carbon-13 chemical shifts were 0.9939 (gas phase), 0.9945 (DMSO), 0.9943 (CCl_4), and 0.9945 ($CHCl_3$), respectively.

The proton chemical shifts of EPM were found by the complete NMR spectra analysis proton and viewed analytically to quantify its various possible effects on the proton shielding constants. Besides, electron-donating atoms or groups improved the shielding and moved the resonance to fewer frequencies. The chemical shift values for hydrogen atoms in methyl groups found and computed were relatively low. Due to shielding effects, all values were lower than three (3) ppm (≤ 3). In this study, the methyl protons at C24 and C42 were shown as a triplet and a singlet with three proton signals at 1.22 and 3.99 ppm, whereas it was calculated that theoretical findings were at 1.05–1.40 ppm and 3.75–4.30 ppm, respectively. Another essential factor is that hydrogen attached or neighboring electron withdrawn from atom or group can reduce the chemical shielding and move up the attached proton's resonance toward a greater frequency. Due to the reasons mentioned above, the N–H proton of the 1,2,4-triazole ring showed a signal at 12.42 ppm and was calculated at 7.50 (gas phase), 8.03 (DMSO), 7.75 (CCl_4), and 7.89 ($CHCl_3$) ppm, respectively. The aromatic proton signals of EPM occurred at 7.13–8.07 ppm and were measured computationally at 6.50–8.50 ppm. The hydrogen (H17) atom could be seen as a doublet of a doublet in the ^{1}H NMR spectrum at 7.47 ppm and was in excellent accordance with the calculated value at 7.88 (gas phase), 7.93 (DMSO), 7.90 (CCl_4), and 7.91 ($CHCl_3$) ppm, respectively. All other chemical shift values and RMSD results are listed in Table 2. As shown in Table 2, the calculated results of ^{1}H and ^{13}C NMR chemical shift value for EPM were closer to the experimental results. The RMSD (root-mean-square deviation) values showed that the H atoms (1.00–1.40 ppm) in solution had better correlations than the C atoms (2.50–2.70 ppm). The correlation diagram between the experimental and computed chemical shifts of proton and carbon-13 NMR analyzed through the B3LYP/6–311++G(d,p) method were displayed in Fig. S2 (Supplementary materials). The regression coefficients of EPM were observed to be 0.8542 (gas phase), 0.8798 (DMSO), 0.8668 (CCl_4), and 0.8737 ($CHCl_3$) for proton chemical shifts. The arrangement between the experimental and computed chemical shift values was great for carbon-13 NMR but less for proton NMR due to the acidic character of the N–H proton.

$\delta_{exp\ (ppm)} = 0.9564\ \delta_{calc} + 1.3063$ ($R^2 = 0.9939$) (gas phase for carbon-13 NMR)

$\delta_{exp\ (ppm)} = 1.0017\ \delta_{calc} + 0.1800$ ($R^2 = 0.8542$) (gas phase for proton NMR)

$\delta_{exp\ (ppm)} = 0.9545\ \delta_{calc} + 1.1586$ ($R^2 = 0.9945$) (DMSO for carbon-13 NMR)

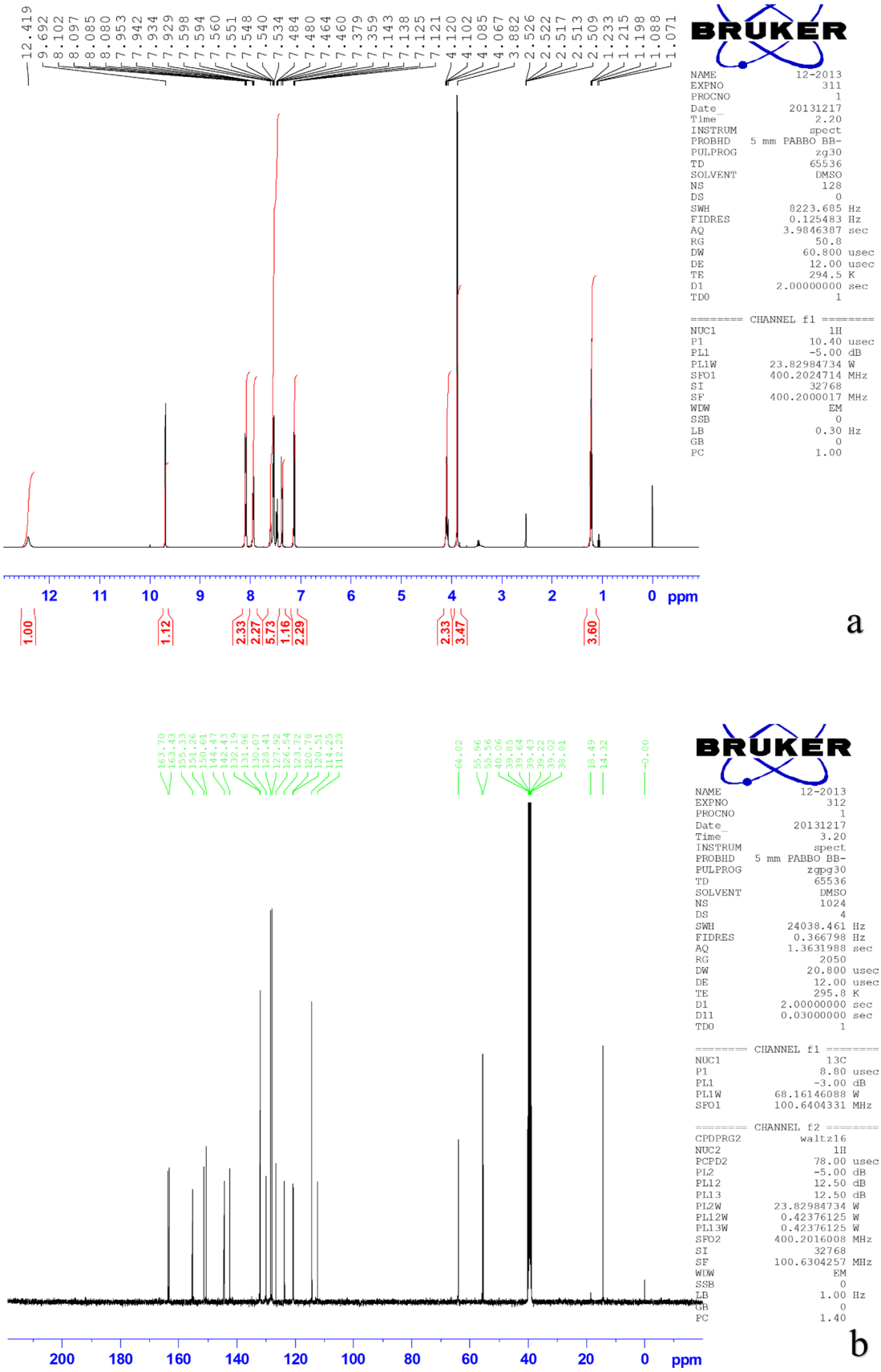

Fig. 5 Observed ^{1}H-NMR (**a**), and ^{13}C-NMR spectra (**b**) of 2-ethoxy-4-[(5-oxo-3-phenyl-1,5-dihydro-1,2,4-triazol-4-ylimino)-methyl]-phenyl-4-methoxybenzoate

Table 2 The calculated and experimental ^{13}C and ^{1}H NMR isotropic chemical shifts of 2-ethoxy-4-[(5-oxo-3-phenyl-1,5-dihydro-1,2,4-triazol-4-ylimino)-methyl]-phenyl-4-methoxybenzoate (with respect to TMS, all values in ppm)

Nucleus	δ_{xp}	$\delta_{cal.}$ (Vacuum)	δ_{diff}	$\delta_{cal.}$ (DMSO)	δ_{diff}	$\delta_{cal.}$ (CCl_4)	δ_{diff}	$\delta_{cal.}$ ($CHCl_3$)	δ_{diff}
29-C	163.70	168.35	− 0.88	170.33	− 1.79	169.20	− 1.25	169.73	− 1.50
14-C	151.26	157.81	1.39	157.61	− 0.04	157.83	0.79	157.77	0.40
8-C	155.33	155.77	− 0.98	156.61	− 0.34	156.17	− 0.79	156.39	− 0.61
2-C	150.61	154.98	5.05	155.99	4.69	155.47	4.86	155.74	4.77
1-C	144.47	152.34	1.08	152.96	0.56	152.63	0.82	152.80	0.68
18-C	142.43	150.26	− 2.54	149.10	− 2.69	149.85	− 2.61	149.52	− 2.66
11-C	132.19	139.26	− 2.58	139.51	− 1.04	139.30	− 2.00	139.37	− 1.57
33-C	131.96	138.65	− 2.30	138.67	− 2.13	138.67	− 2.16	138.67	− 2.12
32-C	131.96	137.44	− 1.95	137.30	− 1.56	137.41	− 1.78	137.37	− 1.68
47-C	128.41	134.21	− 0.80	135.48	− 0.25	134.74	− 0.59	135.09	− 0.43
53-C	130.07	135.09	− 1.26	135.24	− 2.07	135.13	− 1.59	135.17	− 1.81
48-C	128.41	132.74	− 0.44	133.48	− 0.17	133.05	− 0.30	133.26	− 0.22
46-C	132.41	133.45	0.15	132.84	− 0.15	133.26	0.03	133.09	− 0.06
51-C	127.92	131.78	3.47	132.81	4.46	132.15	3.83	132.44	4.10
49-C	127.92	133.14	0.58	132.41	0.00	132.83	0.40	132.63	0.23
16-C	123.72	128.66	− 0.72	128.57	0.38	128.62	− 0.25	128.59	0.05
31-C	120.73	126.11	− 0.64	124.44	− 0.16	125.43	− 0.43	124.98	− 0.29
34-C	114.25	122.34	− 1.19	122.76	0.79	122.50	− 0.37	122.61	0.17
13-C	120.51	120.16	− 4.06	119.96	− 4.09	120.02	− 4.05	119.96	− 4.06
12-C	112.23	118.13	4.29	119.85	4.85	118.86	4.58	119.33	4.73
36-C	114.25	110.35	− 2.06	112.65	− 3.33	111.24	− 2.60	111.88	− 2.94
21-C	64.02	65.91	7.40	66.50	5.56	66.16	6.71	66.32	6.19
42-C	55.56	56.06	− 0.32	56.78	− 0.61	56.35	− 0.46	56.56	− 0.54
24-C	14.32	15.02	0.64	14.93	0.20	14.94	0.45	14.92	0.33
RMSD		**2.69**		**2.55**		**2.60**		**2.56**	
9-H	9.69	10.51	− 1.35	10.49	− 1.09	10.50	− 1.24	10.50	− 1.16
35-H	8.09	8.42	− 1.02	8.48	− 0.89	8.45	− 0.97	8.46	− 0.93
50-H	7.94	8.30	− 0.53	8.39	− 0.45	8.33	− 0.50	8.36	− 0.48
37-H	8.09	8.38	− 0.56	8.38	− 0.51	8.38	− 0.54	8.38	− 0.52
52-H	7.94	8.12	− 0.48	8.15	− 0.35	8.14	− 0.43	8.15	− 0.40
4-H	12.42	7.50	− 0.37	8.03	− 0.27	7.75	− 0.34	7.89	− 0.31
17-H	7.47	7.88	4.73	7.93	4.33	7.90	4.53	7.91	4.43
55-H	7.55	7.61	− 0.60	7.81	− 0.52	7.69	− 0.57	7.75	− 0.54
56-H	7.54	7.54	− 0.25	7.78	− 0.32	7.64	− 0.28	7.70	− 0.30
54-H	7.55	7.55	− 0.19	7.77	− 0.29	7.64	− 0.23	7.70	− 0.26
19-H	7.37	7.22	− 0.19	7.39	− 0.28	7.29	− 0.23	7.34	− 0.25
39-H	7.13	7.14	− 0.04	7.26	− 0.08	7.19	− 0.06	7.22	− 0.06
15-H	7.60	6.90	− 0.21	7.22	− 0.18	7.03	− 0.20	7.12	− 0.19
40-H	7.13	6.66	0.51	7.02	0.33	6.81	0.44	6.91	0.39
44-H	3.88	4.14	0.27	4.26	0.06	4.20	0.19	4.23	0.13
22-H	4.09	3.90	− 0.44	4.09	− 0.40	3.97	− 0.43	4.02	− 0.42
43-H	3.88	3.75	0.01	3.94	− 0.02	3.83	0.01	3.88	0.00
23-H	4.09	3.81	− 0.06	3.93	− 0.08	3.87	− 0.06	3.90	− 0.07
45-H	3.88	3.73	0.09	3.92	0.14	3.80	0.11	3.86	0.12
25-H	1.22	1.34	− 0.03	1.32	− 0.06	1.34	− 0.04	1.33	− 0.04
26-H	1.22	1.05	− 0.30	1.26	− 0.09	1.12	− 0.21	1.30	− 0.15
27-H	1.22	1.36	− 0.01	1.25	− 0.03	1.33	0.00	1.18	− 0.13
RMSD		**1.32**		**1.03**		**1.08**		**1.05**	

RMSD Root Mean Square Deviation

$\delta_{exp\ (ppm)} = 1.0095\ \delta_{calc} - 0.0177$ ($R^2 = 0.8798$) (DMSO for proton NMR)
$\delta_{exp\ (ppm)} = 0.9552\ \delta_{calc} + 1.2837$ ($R^2 = 0.9943$) (CCl_4 for carbon-13 NMR)
$\delta_{exp\ (ppm)} = 1.0070\ \delta_{calc} + 0.0848$ ($R^2 = 0.8668$) (CCl_4 for proton NMR)
$\delta_{exp\ (ppm)} = 0.9548\ \delta_{calc} + 1.2370$ ($R^2 = 0.9945$) ($CHCl_3$ for carbon-13 NMR)
$\delta_{exp\ (ppm)} = 1.0089\ \delta_{calc} + 0{,}0319$ ($R^2 = 0.8737$) ($CHCl_3$ for proton NMR)

Frontier molecular orbitals (FMOs)

The FMOs are of significant importance in optical, electric, and quantic properties, as well as in UV–VIS spectrums**.** The highest occupied molecular orbital (HOMO and HOMO-1) and lowest unoccupied molecular orbital (LUMO and LUMO+1) are known as the frontier orbitals [46, 47]. The energies of HOMO and LUMO are also quite valuable for physicists and chemists and crucial in quantum chemistry. Total energy, dipole moment, and energy gap affect molecular stability. The capacity to donate an electron is called HOMO, in which the capability of obtaining an electron is called LUMO. HOMO, which is considered the outermost orbital with electrons, tends to supply electrons like a donor. LUMO, however, may be considered as the innermost orbital involving free places to accept electrons**.** The HOMO and LUMO are extremely significant quantum chemistry parameters. The electronic absorption is defined as the transfer from the ground into the first excited state and was described primarily by an electron excitement, from the highest molecular orbital occupied to the lower molecular orbital unoccupied [46, 47]. The energy basis sets and distributions of the HOMO, HOMO-1, LUMO, and LUMO+1 for the EPM compound were computed at the B3LYP/6–311++G(d,p) basis set and are indicated in Fig. 6. The HOMO, HOMO-1, LUMO, and LUMO+1 energies for EPM were computed as − 6.162, − 6.480, − 1.908, − 1.449 eV, respectively. The 3D plots of the FMOs (HOMO-1, HOMO, LUMO, and LUMO+1) obtained at B3LYP/6-311G++(d,p) basis set for EPM in the gas phase are shown in Table 3 and Fig. 6. The orbital distributions of phenyl and triazole groups were conjugated through the benzylidene nucleus in the center. Meanwhile, the length of the π-conjugation had increased with the addition of phenyl units. For compound EPM, the highest occupied molecular orbitals (HOMOs) were primarily situated on the triazole and phenyl moiety. In contrast, the lowest unoccupied molecular orbitals (LUMO) shifted to the imine group bounded central phenyl ring. The EPM had the lowest HOMO–LUMO band-gap (4.239 eV), which meant that the π-electron transfer of the EPM was the simplest. However, due to the extensive conjugation of phenyl units, the LUMO of EPM had a lower value. The low-lying LUMO (− 1.908 eV) in EPM enables the faster and more excellent transfer of charge from the donor to the acceptor in the excited state, led to the redshift of a lower HOMO–LUMO band-gap in the absorption spectrum.

The electronic parameters of the molecule were determined by the total energies and the theorem of Koopmans [48]. The HOMO is the orbital that acts mainly as an electron donor, and the LUMO is the most commonly used orbital as the acceptor of the electron. The HOMO–LUMO gap defines optical polarizability, chemical reactivity, and chemical hardness–softness (η and ξ) for the molecule. According to global reactivity descriptors, $IP = -E_{HOMO}$ was used to calculate the ionization potential, and $EA = -E_{LUMO}$ was used to calculate the electron affinity. The computed energy value of these four molecular orbitals, the energy gaps, and specific quantum identifiers such as electrophilicity index (Ψ), chemical potential (μ), electronegativity (χ), chemical hardness (η), and softness (ξ) were computed with B3LYP/6–311++G(d,p) basis set and the outcomes acquired in gas phase are listed in Table 3.

Electronegativity $\chi = (IP + EA)/2$
Chemical potential $\mu = -(IP + EA)/2$
Chemical hardness $\eta = (IP - EA)/2$
Softness $\xi = 1/2\eta$
Electrophilicity index $\Psi = \eta^2/2\eta$

The energy gaps between HOMO and LUMO, HOMO-1 and LUMO, HOMO and LUMO+1, and HOMO-1 and LUMO+1 were 4.253 eV, 4.572 eV, 4.712 eV, and 5.031 eV, respectively. The computed values of electronegativity (χ), chemical potential (μ), chemical hardness (η), softness (ξ), and electrophilicity index (Ψ) were found to be 4.027 eV, − 4.027 eV, 2.122 eV, 1.061 eV, and 3.821 eV, respectively.

Molecular electrostatic potential

The MEP is a pretty useful descriptor for deciding upon the sites of electronic and nucleophilic reactions and the interactions of hydrogen bonding. The electrostatic potential is also ideal for the analysis of procedures relying on the "recognition" of a molecule by another, such as enzyme–substrate relationship and drug-receptor, because the two species first "see" each other with their capacity [49]. The MEP was computed with optimized geometry at the B3LYP/6–311++G(d,p) method to predict reactive nucleophilic or electrophilic attack sites for EPM. The negative areas of the MEP (yellow and red) were connected to electrophilic reactivity, while the positive area (blue) was related to nucleophilic reactivity, as seen in Fig. 7. The negative area was located primarily over

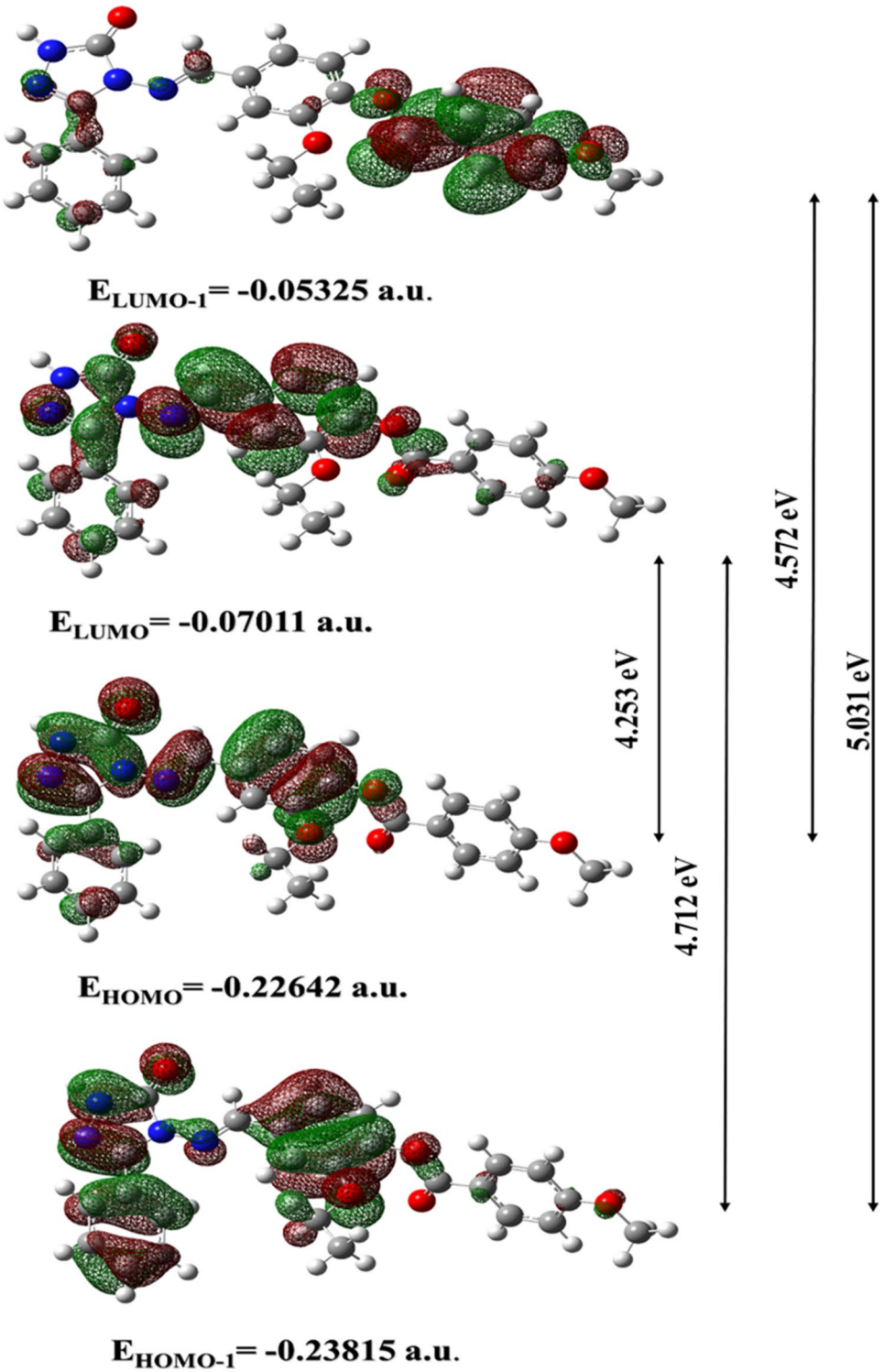

Fig. 6 3D plots of HOMO–1, HOMO, LUMO and LUMO+1 of 2-ethoxy-4-[(5-oxo-3-phenyl-1,5-dihydro-1,2,4-triazol-4-ylimino)-methyl]-phenyl-4-methoxybenzoate on DFT/B3LYP/6–311++G(d,p) level

oxygen atoms (O20, O28, O30, and O41) in carboxyl, ethoxy, and methoxy groups and over carbonyl group between N5 and N6 atoms in the triazole ring. Therefore, the calculations suggest that the area over oxygen atoms (O20, O28, O30, and O41) in carboxyl, ethoxy, and methoxy groups and the area over carbonyl group between N5 and N6 atoms in the triazole ring was a preferred location for electrophilic attacks. However, the N5-H4 bond indicated a potential location for nucleophilic attacks. The MEP map demonstrated that the negative potential locations were located on electronegative atoms and the positive potential locations were around hydrogen atoms. These regions

Table 3 The calculated HOMO–1, HOMO, LUMO, and LUMO+1 energy values, and energy gap between their electronegativity and chemical hardness values of 2-ethoxy-4-[(5-oxo-3-phenyl-1,5-dihydro-1,2,4-triazol-4-ylimino)-methyl]-phenyl-4-methoxybenzoate

Parameters	B3LYP/6–311 + + G(d,p)
E_{HOMO-1} (eV)	− 6.480
E_{HOMO} (eV)	− 6.162
E_{LUMO} (eV)	− 1.908
E_{LUMO+1} (eV)	− 1.449
$E_{HOMO} - E_{LUMO}$ (eV)	4.239
$E_{HOMO} - E_{LUMO+1}$ (eV)	4.712
$E_{HOMO-1} - E_{LUMO}$ (eV)	4.572
$E_{HOMO-1} - E_{LUMO+1}$ (eV)	5.031
χ (Electronegativity) (eV)	4.027
η (Chemical hardness) (eV)	2.122
ξ (Softness) (eV)	1.061
Ψ (Electrophilicity index) (eV)	3.821

provided information regarding the region with which the compound can interact intermolecularly.

Mulliken atomic charges

The Mulliken atomic charge calculation has a significant function in implementing quantum calculations into the molecular system due to dipole moment, atomic charge, electronic structure, molecular polarizability, and molecular system characteristics [50]. The charge distributions over the atoms show that donor and acceptor couples are formed, which involve transferring the charge into the molecule. The population analysis of EPM was determined with the B3LYP/6–311++G(d,p) basis set and displayed in Table S3 (Supplementary Materials). The findings demonstrated the redistribution of the aromatic ring's electron density employing methoxy and ethoxy groups. The load changes with the basis set were caused by polarization. The EPM charge distribution of Fig. 8 indicated that all the hydrogen atoms

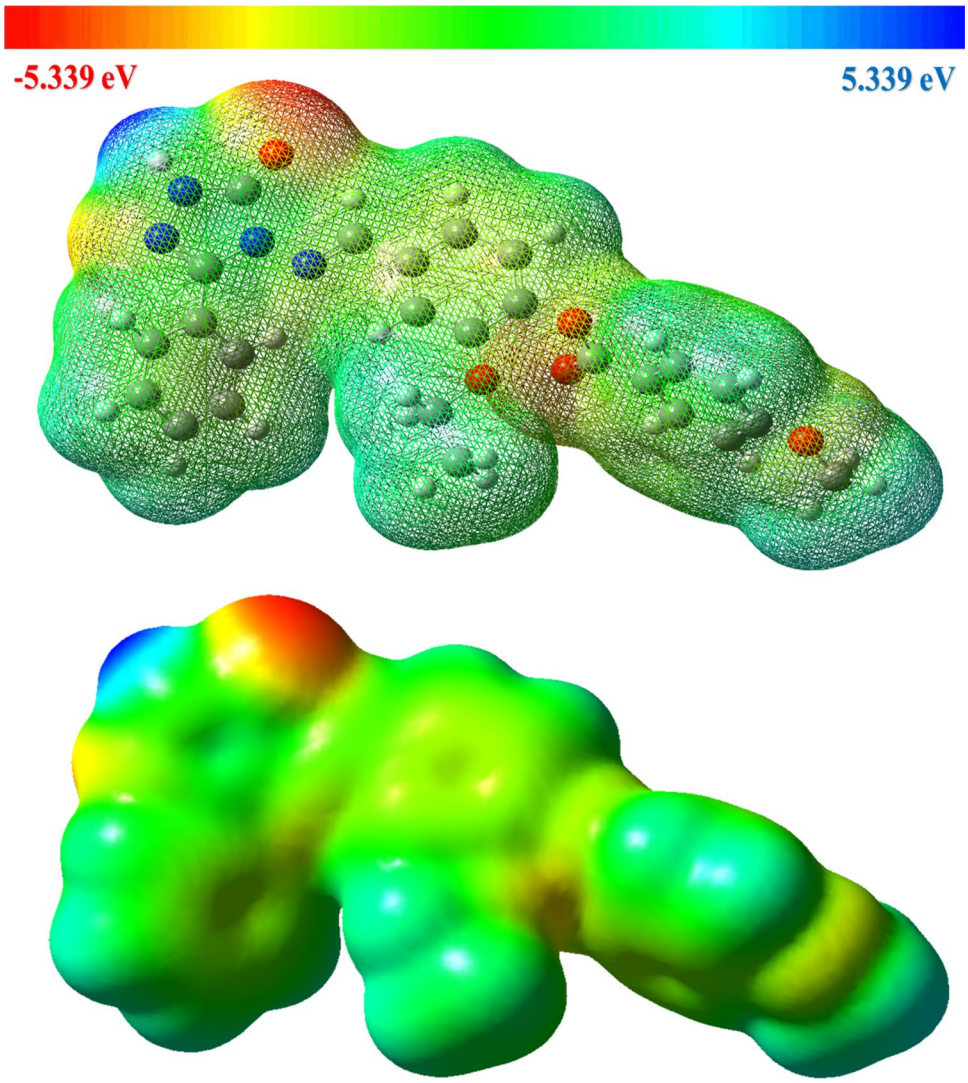

Fig. 7 3D plots of MEP from two different position of view of 2-ethoxy-4-[(5-oxo-3-phenyl-1,5-dihydro-1,2,4-triazol-4-ylimino)-methyl]-phenyl-4-methoxybenzoate on DFT/B3LYP/6–311++G(d,p) level

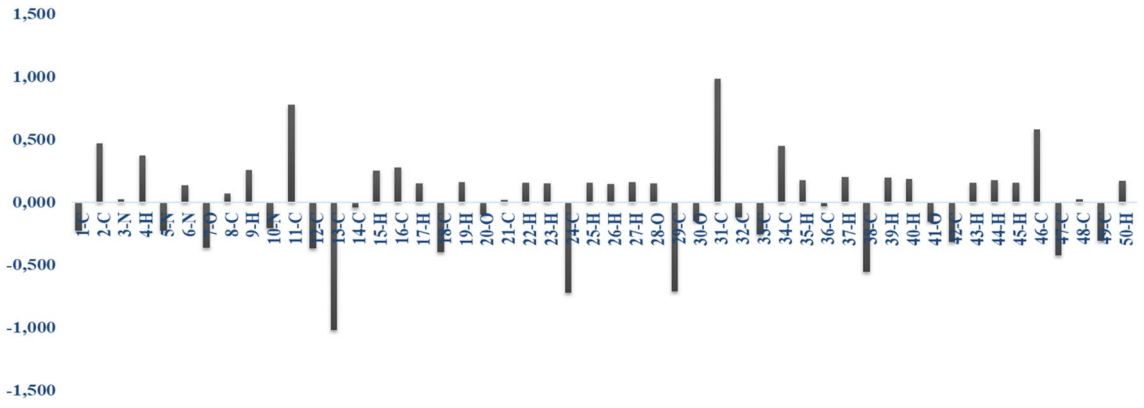

Fig. 8 Mulliken atomic charge graph of 2-ethoxy-4-[(5-oxo-3-phenyl-1,5-dihydro-1,2,4-triazol-4-ylimino)-methyl]-phenyl-4-methoxybenzoate on DFT/B3LYP/6–311++G(d,p) level

were positively charged while the magnitudes of the carbon atomic charge values were positive and negative. The findings indicated that the substitution of the aromatic ring by methoxy, ethoxy groups, and the nitrogen atom caused the redistribution of the molecule's electron density. The maximum positive charges of the C11, C31, C46 atoms in EPM were owing to direct connection of the imine, carboxyl group, and triazole ring. The charge of nitrogen (N) atoms was negative because of its electron-withdrawing nature. All hydrogen atoms had a positive atomic charge, as can be seen in Table S3 (Supplementary Materials). The Mulliken atomic charges show that the O7 atom in triazole and C13, C24, C29, C38, C47, and C19 atoms had bigger negative atomic charges in the gas phase.

UV–vis spectra analysis

The experimentally recorded electronic absorption maximum wavelengths for EPM in ethanol solvent were at 312, 263, and 218 nm, corresponding to the transitions $n \rightarrow \pi^*, \pi \rightarrow \pi^*$, and $n \rightarrow \sigma^*$, respectively. For EPM, time-dependent density functional theory (TD-DFT) was conducted to examine the electronic absorption properties using a completely optimized ground state system. UV–visible spectra analyzed B3LYP/6–311++G(d,p) basis set theoretically, which were used to obtain absorption maximum wavelength values. The computed excitation energies, oscillator strengths (f), and maximum absorption wavelengths (λ) of UV–Vis electron absorption spectroscopy for EPM are given in Table 4. As shown in Table 4, the computed maximum absorption numbers for EPM were 325.54, 309.40, and 297.90 nm. The computed and experimental values were shown to have a good correlation with each other (Table 4).

$\delta_{exp} = 3.377\ \delta_{calc}$ -785.81 ($R^2 = 0.9939$)

Thermodynamic properties

The total energy for a molecule refers to the sum of vibrational, rotational, electronic, and translational energies, i.e., E = Ev + Er + Ee + Et. The statistical thermochemical analysis of EPM was conducted by considering that the molecule should be at the appropriate room temperature for the molecule should be 298.15 K with one atmospheric pressure. The thermodynamic parameters' findings, like zero-point vibrational energy (ZPVE), rotational constant, dipole moment, and SCF energy of EPM, are reported in Table S4 (Supplementary Materials). Based on the vibrational analysis, thermodynamic functions, statistical thermodynamics, entropy (S_m^0), heat capacity (C_p^0), and enthalpy (ΔH_m^0) were

Table 4 The experimental and calculated absorption wavelength (λ), excitation energies, and oscillator strengths (f) of 2-ethoxy-4-[(5-oxo-3-phenyl-1,5-dihydro-1,2,4-triazol-4-ylimino)-methyl]-phenyl-4-methoxybenzoate

Exp. (in ethanol)	Transition	The calculated with B3LYP/6–311++G(d,p) level in vacuum			
λ (nm)/ε (L mol^{-1} cm^{-1})		Transition	λmax (nm)	Excitation energy (eV)	f (oscillator strength)
312 (17,857)	$n \rightarrow \pi^*$,	$H \rightarrow L$	325.54	3.8085	0.4289
263 (30,524)	$\pi \rightarrow \pi^*$	$H-1 \rightarrow L$ $H \rightarrow L+1$	309.40	4.0072	0.0282
218 (33,305)	$n \rightarrow \sigma^*$	$H-1 \rightarrow L+1$ $H \rightarrow L+1$	297.90	4.1620	0.0018

determined at temperatures ranging from 100 to 1000 °K, and the values are illustrated in Table 5. Furthermore, the correlation graphs of temperature dependence are displayed in Fig. 9.

All of these thermodynamic data provide valuable knowledge for more EPM studies. They can be applied in calculating other thermodynamic parameters according to the thermodynamic function relations and taking into account the second law of thermodynamics to determine the path of the chemical reactions.

S_m^0 (cal mol^{-1} K^{-1}) = 0.0001 T^2 + 0,4712 T + 75,494 (R^2 = 0.9999)
C_p^0 (cal mol^{-1} K^{-1}) = -0.0002 T^2 + 0,4246 T + 5,2766 (R^2 = 0.9995)
ΔH_m^0 (kcal mol^{-1}) = 0.0001 T^2 + 0,05 T + 266,95 (R^2 = 0.9995)

Nonlinear optical Properties

Nonlinear optical (NLO) effects are caused by the interaction of electromagnetic areas in different media in order to generate new areas modified from event areas in stage, frequency, or other diffusion characteristics [48]. In the present study, NLO is a success because of its significance in the delivery of important functions such as telecommunications, optical interconnections, and signal processing in fields like frequency change, optical modulation, optical logic, optical switching, and optic storage. The computations of the linear polarizability α, first-order hyperpolarizability β, and the total molecular dipole moment μ of EPM were examined in detail, and DFT was used widely as an efficient method to explore the organic NLO materials. Moreover, the polar characteristics of EPM were computed at the B3LYP/6–311++G(d,p) basis set.

Table 5 Thermodynamic properties at different temperatures of 2-ethoxy-4-[(5-oxo-3-phenyl-1,5-dihydro-1,2,4-triazol-4-ylimino)-methyl]-phenyl-4-methoxybenzoate calculated by B3LYP/6–311++G(d,p) method

T (°K)	S_m^0(cal mol^{-1} K^{-1})	C_p^0(cal mol^{-1} K^{-1})	ΔH_m^0(kcal mol^{-1})
100	121.372	48.565	274.909
200	165.949	80.969	281.383
298.15	205.271	114.453	290.966
300	205.987	115.086	291.179
400	244.457	147.696	304.342
500	283.780	175.151	321.319
600	315.149	198.084	339.274
700	350.348	215.936	360.718
800	377.532	231.132	382.421
900	405.741	243.386	406.165
1000	431.031	253.624	432.141

The result of the calculation of the polarizability and hyperpolarizability tensors (α_{xx}, α_{xy}, α_{yy}, α_{xz}, α_{yz}, α_{zz} and β_{xxx}, β_{xxy}, β_{xyy}, β_{yyy}, β_{xxz}, β_{xyz}, β_{yyz}, β_{xzz}, β_{yzz}, β_{zzz}) was provided through the use of the Gaussian frequency output file. The values (α and β) of Gaussian output, on the other hand, were in atomic units (a.u.) and had been converted to electronic units (esu and Å^3) (α; 1 a.u. = 0.1482×10^{-24} esu 1 au^3 = $(0.529)^3$ Å^3, and β; 1 a.u. = 8.641×10^{-33} esu). The mean polarizability (α), average value of the first hyperpolarizabiliy ($\langle\beta\rangle$), and the anisotropy of polarizability (Δα) can be calculated by utilizing below equations;

$$\alpha_{Total} = \frac{1}{3}\left(\alpha_{xx} + \alpha_{yy} + \alpha_{zz}\right)$$

$$\Delta_\alpha = \frac{1}{\sqrt{2}}\left[\left(\alpha_{xx} - \alpha_{yy}\right)^2 + \left(\alpha_{yy} - \alpha_{zz}\right)^2 + \left(\alpha_{zz} - \alpha_{xx}\right)^2 + 6\alpha_{xz}^2 + 6\alpha_{xy}^2 + 6\alpha_{yz}^2\right]^{\frac{1}{2}}$$

$$\beta_0 = \left[\left(\beta_{xxx} + \beta_{xyy} + \beta_{xzz}\right)^2 + \left(\beta_{yyy} + \beta_{yzz} + \beta_{yxx}\right)^2 + \left(\beta_{zzz} + \beta_{zxx} + \beta_{zyy}\right)^2\right]^{\frac{1}{2}}$$

$$\mu_{Total} = \left(\mu_x^2 + \mu_y^2 + \mu_z^2\right)^{\frac{1}{2}}$$

Based on the present computations, the mean polarizability and dipole moment of EPM were observed to be 8.333 a.u. (56.2250×10^{-24} cm^5/esu) and 3.5738 D (Table 6). The μ_x variable was shown to have the highest dipole moment value which was equal to 3.5687 D. In this respect, the first static hyperpolarizability calculated β value was found to be 6.5662×10^{-30} esu (Table 6).

Urea is one of the prototypes used to explore NLO characteristics of molecular system. It was therefore often used in comparative terms as a threshold value. The estimated values of α_{Total} and β_{Total} for EPM were 56.2250×10^{-24} cm^5/esu and 6.5662×10^{-30} cm^5/esu which had higher range of urea, (0.1947×10^{-30} cm^5/esu) obtained from B3LYP/6–311++G(d,p). The EPM can be a prospective candidate in developing NLO products depending on the magnitude of the first hyper-polarizability. The estimated β value was approximately 34 times that of urea (0.1947×10^{-30} cm^5/esu). The high β value determined through the B3LYP method indicated that EPM was a strong NLO material. Theoretical β component computations are extremely useful because they clearly demonstrate the direction of charge delocalization. To explain this phenomenon within the context of molecular orbital forms, the molecular HOMOs and LUMOs of

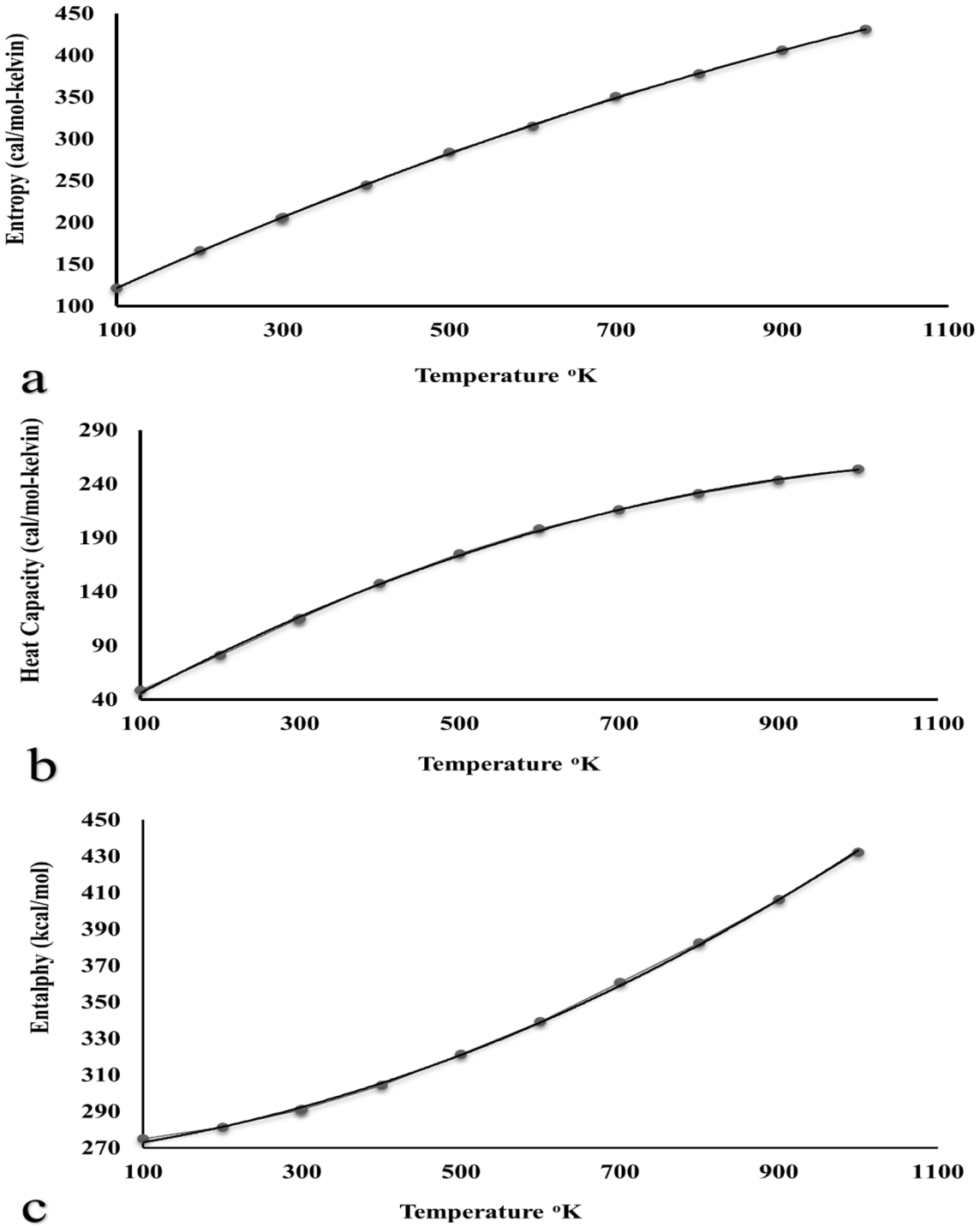

Fig. 9 Correlation graphs for 2-ethoxy-4-[(5-oxo-3-phenyl-1,5-dihydro-1,2,4-triazol-4-ylimino)-methyl]-phenyl-4-methoxybenzoate (**a**) entropy and temperature, (**b**) heat capacity and temperature, (**c**) enthalpy and temperature

EPM, shown in Fig. 6, were examined. The energy gaps (HOMO–LUMO) were computed as 4.253 eV for EPM and 6.569 eV for urea through the same method. As shown in the βtot values for EPM, the greater value of the first hyper-polarizability refers to the reduced HOMO–LUMO

Table 6 The total energy $\mathbf{E_{total}}$ (Hartree), the electric dipole moment $\boldsymbol{\mu}$ (Debye), the average polarizability $\boldsymbol{\alpha_{total}}$ (10^{-24} cm^5/esu), and first hyperpolarizability $\boldsymbol{\beta_{total}}$ (10^{-30} cm^5/esu) of 2-ethoxy-4-[(5-oxo-3-phenyl-1,5-dihydro-1,2,4-triazol-4-ylimino)-methyl]-phenyl-4-methoxybenzoate

	B3LYP
E_{total}	− 1561.4231
μx	3.5687
μy	− 0.1692
μz	− 0.0933
$\mu Toplam$	3.5738
αxx	52.4450
αxy	− 2.0712
αyy	49.6355
αxz	− 0.096
αyz	− 0.05480
αzz	20.1135
α_{total}	56.2250
$\Delta\alpha$ *(esu)*	41.2937
βxxx	− 2452,5725
βxxy	293,7622
βxyy	− 214,0781
βyyy	− 322,4670
βxxz	308,7505
βxyz	− 47,3116
βyyz	3,9081
βxzz	70,5513
βyzz	− 90,3061
βzzz	− 32,3389
β_{total}	6.5662

gaps. This relation revealed the previously reported inverse correlation [51, 52].

Conclusions

In the present study, synthesis and characterization of a novel Schiff base, 2-ethoxy-4-[(5-oxo-3-phenyl-1,5-dihydro-1,2,4-triazol-4-ylimino)-methyl]-phenyl-4-methoxybenzoate (EPM) that contain 1,2,4-triazole ring was accomplished. The EPM's characterization was conducted through infrared spectroscopy, (IR) $^1H/^{13}C$ nuclear magnetic resonance (NMR), and UV–vis analysis. A novel Schiff base, 2-ethoxy-4-[(5-oxo-3-phenyl-1,5-dihydro-1,2,4-triazol-4-ylimino)-methyl]-phenyl-4-methoxybenzoate (EPM), was obtained with significant spectroscopic findings and a yield of 98.71%. Additionally, the newly synthesized compound, EPM, was studied for its *in* vitro potential antioxidant properties with three different methods. In this respect, the metal chelating activity of EPM and standards was observed to decrease in the order of EDTA > EPM > α-tocopherol. A complete vibrational analysis of 2-ethoxy-4-[(5-oxo-3-phenyl-1,5-dihydro-1,2,4-triazol-4-ylimino)-methyl]-phenyl-4-methoxybenzoate (EPM) were conducted through the method of DFT-B3LYP with 6–311++G(d,p) basis set. In this respect, FT-IR spectra of EPM were recorded, and detailed vibrational assignments were obtained. The processes, including molecular geometry, vibrational frequencies, infrared intensities, and Raman scattering activities for EPM, were determined through the use of DFT. The computed HOMO and LUMO energies suggested that the charge transfer took place within the molecule. The ^1H and ^{13}C NMR spectroscopic change values were paired up with the results of the experiments. Besides, all the vibrational frequencies were computed and experimentally obtained FT-IR spectra were also used in the comparison. It was realized that the observed and the computed frequencies were in close agreement. Maximum absorption wavelengths for EPM were also computed via the TD-DFT method. Furthermore, urea was used as a prototypical molecule in the studies focusing upon NLO properties of molecular systems. The title compound (EPM) displayed such a good NLO property that it was 34 times as great as the property of urea. As a result, this chromophore was thought to be a potential building block for nonlinear optical materials. Mulliken atomic charges were also computed, which helped to understand the atomic theory. Besides, the zero-point vibrational energy (ZPVE), rotational constant, dipole moment, SCF energy, and thermodynamic properties of EPM were conducted. The thermodynamic results revealed that the entropies, enthalpies, and heat capacities went up as temperature rose due to intensities of the molecular vibrations rising as a consequence of increasing temperature.

Supplementary Information The online version contains supplementary material available at https://doi.org/10.1007/s13738-021-02401-x.

Acknowledgements The numerical calculations which were exhibited in the present study were completely carried out at TUBITAK ULAKBIM, High Performance and Grid Computing Center (TRUBA resources). It would be a great pleasure to thank to Haydar YUKSEK for his technical support and contributions to the present study.

Authors' Contributions HM carried out all experiments and antioxidant activity and wrote the manuscript and supervised the project. Haydar YÜKSEK provided the technical support.

Funding There were no funding sources for the reported research.

Data availability Not applicable.

Code availability ChemDraw Ultra 8.0, Gaussian 0.9, GaussView 5.0, Veda 4, Chemcraft 1.8.

Declarations

Conflict of interests The author declares that I have not known competing financial interests or personal relationships that could have appeared to influence the work reported in this paper. The paper is original and is not published previously in whole or partially and not being considered elsewhere.

References

1. E.M. Abdelrehim, ACS Omega **6**, 1687 (2021)
2. K.B.H. Salah, M. Maingot, A.-L. Blayo, C. M'Kadmi, M. Damian, S. Mary, S. Cantel, J. Neasta, C. Oiry, S. Péraldi-Roux, G. Fernandez, G.G. Romero, M. Perello, J. Marie, J.-L. Banères, J.-A. Fehrentz, S. Denoyelle, J. Med. Chem. **63**, 10796 (2020)
3. A.S. Al-Ali, D. Khan, A. Naqvi, F.F. Al-blewi, N. Rezki, M.R. Aouad, M. Hagar, ACS Omega **6**, 301 (2021)
4. T. Plech, M. Wujec, U. Kosikowska, A. Malm, B. Rajtar, M. Polz-Dacewicz, Eur. J. Med. Chem. **60**, 128 (2013)
5. İ Küçükgüzel, ŞG. Küçükgüzel, S. Rollas, G. Ötük-Sanış, O. Özdemir, İ Bayrak, T. Altuğ, J.P. Stables, Il Farmaco **59**, 893 (2004)
6. İ Küçükgüzel, E. Tatar, ŞG. Küçükgüzel, S. Rollas, E. De Clercq, Eur. J. Med. Chem. **43**, 381 (2008)
7. O. Grytsai, O. Valiashko, M. Penco-Campillo, M. Dufies, A. Hagege, L. Demange, S. Martial, G. Pagès, C. Ronco, R. Benhida, Bioorganic. Chem. **104**, 104271 (2020)
8. J. Ahirwar, D. Ahirwar, S. Lanjhiyana, A.K. Jha, D. Dewangan, H. Badwaik, J. Heterocycl. Chem. **55**, 2598 (2018)
9. H.M. Aly, M.E. Moustafa, M.Y. Nassar, E.A. Abdelrahman, J. Mol. Struct. **1086**, 223 (2015)
10. M.Y. Nassar, H.M. Aly, E.A. Abdelrahman, M.E. Moustafa, J. Mol. Struct. **1143**, 462 (2017)
11. M.Y. Nassar, H.M. Aly, M.E. Moustafa, E.A. Abdelrahman, J. Inorg. Organomet. Polym. **27**, 1220 (2017)
12. L.H. Al-Wahaibi, J. Joubert, O. Blacque, N.H. Al-Shaalan, A.A. El-Emam, Sci. Rep. **9**, 19745 (2019)
13. R. Ustabaş, N. Süleymanoğlu, Y. Ünver, and Ş. Direkel, Journal of Molecular Structure **1214**, 128217 (2020).
14. R.J. Xavier, E. Gobinath, Spectrochim. Acta Part A Mol. Biomol. Spectrosc. **86**, 242 (2012)
15. H. Medetalibeyoğlu, H. Yüksek, Bul. Chem. Commun. **49**, 78 (2017)
16. I.E. Mikhailov, G.A. Dushenko, M.E. Gurskii, N.I. Vikrischuk, L.D. Popov, Y.V. Revinskii, K.A. Lyssenko, V.I. Minkin, Polyhedron **166**, 73 (2019)
17. Y. Sert, S. Lahmidi, M. El Hafi, H. Gökce, E.M. Essassi, A. Ejjoumamany, J.T. Mague, J. Mol. Struct. **1206**, 127680 (2020)
18. M. Gökalp, B. Dede, T. Tilki, Ç.K. Atay, J. Mol. Struct. **1212**, 128140 (2020)
19. M. Saleem, M. Rafiq, Y.K. Jeong, D.W. Cho, C.-H. Kim, S.-Y. Seo, C.-S. Choi, S.-K. Hong, K.H. Lee, Med. Chem. **14**, 451 (2018)
20. M. Fizer, M. Slivka, N. Korol, O. Fizer, J. Mol. Struct. **1223**, 128973 (2021)
21. S. An, S. Meng, J. Xue, H. Wang, X. Zheng, Y. Zhao, Spectrochim. Acta Part A Mol. Biomol. Spectrosc. **258**, 119762 (2021)
22. N. Korol, M. Slivka, M. Fizer, V. Baumer, V. Lendel, Monatsh. Chem. **151**, 191 (2020)
23. A.O. Ortolan, I. Øestrøm, G.F. Caramori, R.L.T. Parreira, A. Muñoz-Castro, F.M. Bickelhaupt, Organometallics **37**, 2167 (2018)
24. O.M.I. Adly, A. Taha, M.A. Ibrahim, S.A. Fahmy, Appl. Organ. Chem. **34**, e5763 (2020)
25. M. Oyaizu, Japan J. Nutr. **44**, 307 (1986)
26. M.S. Blois, Nature **181**, 1199 (1958)
27. P.-D. Duh, Y.-Y. Tu, G.-C. Yen, LWT Food Sci. Technol. **32**, 269 (1999)
28. T.C.P. Dinis, V.M.C. Madeira, L.M. Almeida, Arch. Biochem. Biophys. **315**, 161 (1994)
29. F. Yamaguchi, T. Ariga, Y. Yoshimura, H. Nakazawa, J. Agric. Food Chem. **48**, 180 (2000)
30. M.J. Frisch, G.W. Trucks, H.B. Schlegel, G.E. Scuseria, M.A. Robb, J.R. Cheeseman, G. Scalmani, V. Barone, B. Mennucci, G.A. Petersson, H. Nakatsuji, M. Caricato, X. Li, H.P. Hratchian, A.F. Izmaylov, J. Bloino, G. Zheng, J.L. Sonnenberg, M. Hada, M. Ehara, K. Toyota, R. Fukuda, J. Hasegawa, M. Ishida, T. Nakajima, Y. Honda, O. Kitao, H. Nakai, T. Vreven, J.A. Montgomery Jr., J.E. Peralta, F. Ogliaro, M. Bearpark, J.J. Heyd, E. Brothers, K.N. Kudin, V.N. Staroverov, R. Kobayashi, J. Normand, K. Raghavachari, A. Rendell, J.C. Burant, S.S. Iyengar, J. Tomasi, M. Cossi, N. Rega, J.M. Millam, M. Klene, J.E. Knox, J.B. Cross, V. Bakken, C. Adamo, J. Jaramillo, R. Gomperts, R.E. Stratmann, O. Yazyev, A.J. Austin, R. Cammi, C. Pomelli, J.W. Ochterski, R.L. Martin, K. Morokuma, V.G. Zakrzewski, G.A. Voth, P. Salvador, J.J. Dannenberg, S. Dapprich, A.D. Daniels, Ö. Farkas, J.B. Foresman, J.V. Ortiz, J. Cioslowski, D.J. Fox, *Gaussian 09* (Gaussian Inc, Wallingford CT, 2009)
31. R. D. Dennington, T. A. Keith, and J. M. Millam GaussView 5.0.8, Gaussian (2008).
32. A.D. Becke, J. Chem. Phys. **98**, 5648 (1993)
33. C. Lee, W. Yang, R.G. Parr, Phys. Rev. B **37**, 785 (1988)
34. A.P. Scott, L. Radom, J. Phys. Chem. **100**, 16502 (1996)
35. J. Foresman and A. Frisch, *Exploring Chemistry With Electronic Structure Methods, 3rd Edition* (2015).
36. M.H. Jamróz, Spectrochim. Acta Part A Mol. Biomol. Spectrosc. **114**, 220 (2013)
37. K. Wolinski, J.F. Hinton, P. Pulay, J. Am. Chem. Soc. **112**, 8251 (1990)
38. R. Moreno-Fuquen, M.M. Hincapié-Otero, D. Becerra, J.-C. Castillo, J. Portilla, M.A. Macías, J. Mol. Struct. **1226**, 129317 (2021)
39. S. Wu, W. Zhang, L. Qi, Y. Ren, H. Ma, J. Mol. Struct. **1197**, 171 (2019)
40. A. Karayel, S. Özbey, C. Kuş, G. Ayhan-Kılcıgil, J. Mol. Struct. **1177**, 476 (2019)
41. B.H. Stuart, *Infrared Spectroscopy: Fundamentals and Applications* (Wiley, New York, 2004)
42. D.L. Pavia, G.M. Lampman, G.S. Kriz, J.A. Vyvyan, *Introduction to Spectroscopy*, 5th edn. (Cengage Learning, Stamford, 2014)
43. L. Bellamy, *The Infra-Red Spectra of Complex Molecules* (Springer, Netherlands, 1975)
44. R.M. Silverstein, F.X. Webster, D.J. Kiemle, D.L. Bryce, *Spectrometric Identification of Organic Compounds* (Wiley, New York, 2014)
45. P. Pulay and J. F. Hinton, in *EMagRes* (American Cancer Society, 2007).
46. K. Fukui, Science **218**, 747 (1982)
47. P. Atkins and J. de Paula, *Physical Chemistry for the Life Sciences*, 2nd edition (W. H. Freeman, New York : Oxford, 2011).
48. J. Luo, Z.Q. Xue, W.M. Liu, J.L. Wu, Z.Q. Yang, J. Phys. Chem. A **110**, 12005 (2006)
49. J.S. Murray, K. Sen, *Molecular Electrostatic Potentials: Concepts and Applications* (Elsevier Science, Amsterdam, 1996)
50. R.S. Mulliken, J. Chem. Phys. **23**, 1841 (1955)
51. R. Shukla, T.P. Mohan, B. Vishalakshi, D. Chopra, CrystEngComm **16**, 1702 (2014)
52. M. Nadeem, U. Yunus, M.H. Bhatti, K. Ayub, M. Mehmood, M.J. Saif, J. Phys. Chem. Solids **110**, 218 (2017)
53. L. Gavara, L. Sevaille, F. De Luca, P. Mercuri, C. Bebrone, G. Feller, A. Legru, G. Cerboni, S. Tanfoni, D. Baud, G. Cutolo, B. Bestgen, G. Chelini, F. Verdirosa, F. Sannio, C. Pozzi, M. Benvenuti, K. Kwapien, M. Fischer, K. Becker, J.-M. Frère, S. Mangani, N. Gresh, D. Berthomieu, M. Galleni, J.-D. Docquier, and J.-F. Hernandez, Eur. J. Med. Chem. **208**, 112720 (2020).
54. M.M. Slaihim, F.S.R. Al-Suede, M. Khairuddean, M.B.K. Ahamed, A.M.S.A. Majid, J. Mol. Struct. **1196**, 78 (2019)